

Supporting Information

Halogen-bond-based cooperative ion-pair recognition by an crown-ether-embedded 5-iodo-1,2,3-triazole

Ronny Tepper,^{a, b} Benjamin Schulze,^{a, b} Peter Bellstedt,^{a, c} Jan Heidler,^{a, b} Helmar Görls,^c
Michael Jäger,^{a, b} and Ulrich S. Schubert^{a, b, *}

^a Laboratory of Organic and Macromolecular Chemistry (IOMC), Friedrich Schiller University Jena, Humboldtstr. 10, 07743 Jena, Germany

^b Jena Center for Soft Matter (JCSM), Friedrich Schiller University Jena, Philosophenweg 7, 07743 Jena, Germany

^c Laboratory of Inorganic and Analytical Chemistry, Friedrich Schiller University Jena, Humboldtstr. 8, 07743 Jena, Germany

E-mail: ulrich.schubert@uni-jena.de.

Table of Contents:

1. Experimental section:	2
2. NMR spectra:	8
3. NMR analysis:	19
4. Molecular structures:	39
5. Theoretical studies:	43
6. References:	46

1. Experimental section:

General Experimental Methods:

All starting materials were purchased from commercial suppliers and used as obtained unless otherwise specified. Commercially available (5-chloro-1-pentynyl)trimethylsilane was used to prepare the more reactive (5-iodo-1-pentynyl)trimethylsilane.¹ Tetrahydrofuran (THF) was dried and degassed with the help of a solvent purification system and kept under nitrogen using standard Schlenk techniques. A programmable syringe pump from WPI was used as the continuous addition system to perform the CuAAC cyclization under pseudo-high-dilution conditions. NMR spectra were measured on spectrometer at 250, 300, 400, 500, or 600 MHz in deuterated solvents at 25 °C. Chemical shifts were reported in ppm by using the solvent as an internal standard. Electrospray ionization (ESI)-MS spectra were measured on an ESI-(Q)-TOF-MS mass spectrometer equipped with an automatic syringe pump for sample injection. The mass spectrometer was operating in the positive-ion mode and the standard ESI source was used to generate the ions. Flash column chromatography was carried out on a Biotage Isolera One System using Biotage SNAP Cartridges KP-Sil.

Crystal structure determination:

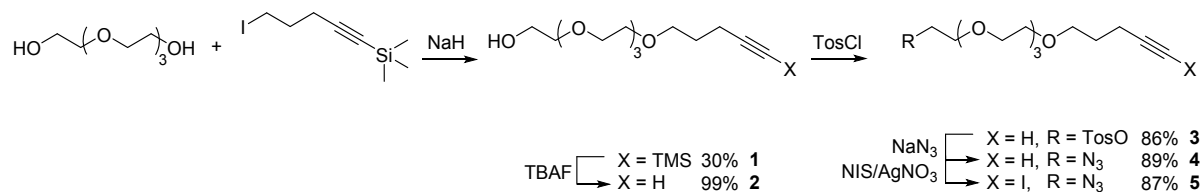
The intensity data for the compounds were collected on a Nonius Kappa CCD diffractometer using graphite-monochromated Mo-K α radiation. Data were corrected for Lorentz and polarization effects; absorption was taken into account on a semi-empirical basis using multiple-scans.²⁻⁴ The structures were solved by direct methods (SHELXS⁵) and refined by full-matrix least squares techniques against Fo² (SHELXL-97⁵ and SHELXL-2014⁶). All hydrogen atoms bounded to the compounds **7**, **7** × NaBPh₄ and bounded to the water molecules of **7** × NaI were located by difference Fourier synthesis and refined isotropically. All other hydrogen atoms were included at calculated positions with fixed thermal parameters. All non-hydrogen, non-disordered atoms were refined anisotropically.^{5,6} The crystal of **6** and **6** × NaPF₆ were a partial-merohedral twins. The twin laws were determined by PLATON.⁷ The contribution of the main components were refined to 0.726(4), and 0.676 (8) respectively. Crystallographic data as well as structure solution and refinement details are summarized in **Table S 3**. MERCURY-3.3 was used for structure representations.

Computational details:

The theoretical calculations were performed using density functional theory (DFT). All calculations were performed with the Gaussian09 program package (Version A.02).⁸ The hybrid functional m062x⁹ has been selected in combination with the QZVP basis set¹⁰ for all atoms except for I, which was described by an effective core potential and the associated orbitals (mwb). The calculations were performed in the gas phase (optimization criterion ‘tight’, integration grid ‘ultrafine’), and the true minimum of the optimized geometries was confirmed by vibrational analysis showing no imaginary frequencies. The graphical visualizations were generated by GaussView5.0.8,¹¹ *i.e.* the iso-values for the electrostatic potentials were optimized for visualization (see **Figure S 49** and **Figure S 50**).

Synthetic Procedures:

Scheme S 1: Schematic representation of the synthesis of the acyclic precursor.



2,2-Dimethyl-8,11,14,17-tetraoxa-2-silanonadec-3-yn-19-ol (**1**)

Sodium hydride (0.37 g, 15.40 mmol, 1.1 eq.) was added in small portions to a stirred solution of tetraethylene glycol (7.61 g, 39.2 mmol, 2.8 eq.) in 110 mL dry THF maintained at 0 °C in an inert atmosphere. After 1 h the hydrogen evolution was entirely completed and a solution of (5-iodo-1-pentynyl)trimethylsilane¹ (3.73 g, 14.0 mmol) in 10 mL dry THF was added dropwise at 0 °C. The mixture was slowly warmed to room temperature and stirred overnight, whereupon a clear yellowish solution was formed. After neutralization of residual sodium hydride by addition of 20 mL water, the mixture was concentrated *in vacuo*. The residue was redissolved in CH₂Cl₂ and washed with water. The organic fraction was dried over sodium sulfate, filtered, and was again concentrated *in vacuo*. The crude product was purified by column chromatography (silica, CH₂Cl₂ to CH₂Cl₂/methanol (98:2)) to obtain the desired product **1** as yellowish oil in poor yield (1.38 g, 30%). Noteworthy, partial removal of the TMS group was observed during the reaction. ¹H NMR (300 MHz, CD₃CN) δ = 3.64 - 3.42 (m, 18H), 2.79 (t, ³J = 5.8 Hz, 1H), 2.27 (t, ³J = 7.1 Hz, 2H), 1.69 (p, ³J = 6.7 Hz, 2H), 0.12 (s, 9H) ppm. ¹³C NMR (63 MHz, CD₃CN) δ = 108.1, 85.3, 73.3, 71.2, 71.2, 71.1, 71.1, 70.9, 70.0, 62.0, 29.5, 17.0, 0.2 ppm. HRMS (ESI-TOF): m/z = [M + Na⁺]⁺ Calcd for C₁₆H₃₂O₅SiNa 355.1911, Found 355.1906.

3,6,9,12-Tetraoxaheptadec-16-yn-1-ol (**2**)

Tetrabutyl ammonium fluoride (TBAF) (1.03 g, 3.69 mmol, 2 eq.) in 2 mL THF was added to a solution of **1** (613 mg, 1.84 mmol) in 3 mL MeOH and stirred at room temperature overnight. After removal of the solvents *in vacuo* the residue was taken up in CH₂Cl₂, washed with water and was again concentrated *in vacuo* to obtain the desired product **2** as yellowish oil in quantitative yields (480 mg, 99%). ¹H NMR (300 MHz, CDCl₃) δ = 3.77 - 3.50 (m, 18H), 2.35 - 2.24 (m, 3H), 1.93 (t, ⁴J = 2.5 Hz, 1H), 1.80 (p, ³J = 6.6 Hz, 2H) ppm. ¹³C NMR (63 MHz, CDCl₃) δ = 84.2, 72.7, 70.8, 70.8, 70.7, 70.5, 70.4, 69.7, 68.6, 61.9, 28.6, 15.3 ppm. HRMS (ESI-TOF): m/z = [M + Na⁺]⁺ Calcd for C₁₃H₂₄O₅Na 283.1516, Found 283.1524.

3,6,9,12-Tetraoxaheptadec-16-yn-1-yl 4-methylbenzenesulfonate (3)

2 (500 mg, 1.92 mmol) and *N,N*-dimethylpyridin-4-amine (DMAP) (23.5 mg, 0.19 mmol, 0.1 eq.) were placed in an inert atmosphere. Subsequently, 50 mL dry CH₂Cl₂ and NEt₃ (0.4 mL, 2.88 mmol, 1.5 eq.) were added and the resulting solution was cooled to 0 °C. *p*-Toluenesulfonyl chloride (TosCl) (549 mg, 2.88 mmol, 1.5 eq.) was added slowly and the reaction was slowly warmed to room temperature and stirred overnight. The crude reaction mixture was quenched with 25 mL water and extracted with CH₂Cl₂. The combined organic layers were dried over sodium sulfate, filtered, and concentrated *in vacuo*. The crude oil was purified by a short column chromatography (silica, CH₂Cl₂ to CH₂Cl₂/methanol (95:5)) to obtain the desired product **3** as yellowish oil in very good yields (683 mg, 86%). ¹H NMR (250 MHz, CDCl₃) δ = 7.79 (d, ³J = 8.3 Hz, 2H), 7.33 (d, ³J = 8.0 Hz, 2H), 4.15 (t, ³J = 4.5 Hz, 2H), 3.74 - 3.48 (m, 16H), 2.44 (s, 3H), 2.27 (td, ⁴J = 2.6 Hz, ³J = 7.1 Hz, 2H), 1.93 (t, ⁴J = 2.7 Hz, 1H), 1.78 (p, ³J = 6.7 Hz, 2H) ppm. ¹³C NMR (63 MHz, CDCl₃) δ = 144.9, 133.2, 129.9, 128.1, 84.1, 70.9, 70.8, 70.7, 70.7, 70.7, 70.4, 69.7, 69.4, 68.8, 68.6, 28.7, 21.8, 15.3 ppm. HRMS (ESI-TOF): *m/z* = [M + Na⁺]⁺ Calcd for C₂₀H₃₀O₇SNa 437.1604, Found 437.1593.

1-Azido-3,6,9,12-tetraoxaheptadec-16-yne (4)

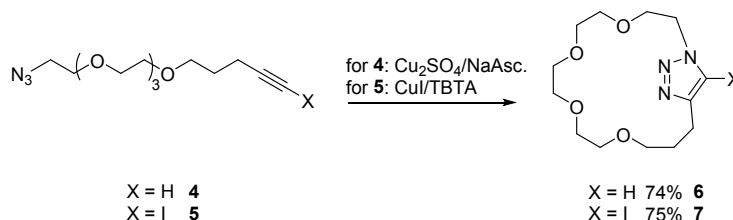
Sodium azide (72 mg, 1.11 mmol, 4 eq.) was added to a solution of **3** (114 mg, 0.28 mmol) in 5 mL anhydrous DMSO. The mixture was stirred in an inert atmosphere for two days at room temperature in the dark. Subsequently, water was added and the mixture was extracted with diethyl ether. The combined organic layers were dried over sodium sulfate, filtered, and concentrated *in vacuo* to obtain the desired product **4** as yellowish oil in very good yields (70 mg, 89%). To avoid any unwanted click coupling, the reaction and the purification steps were performed at room temperature and the product was stored in the fridge. ¹H NMR (300 MHz, CDCl₃) δ = 3.78 - 3.46 (m, 16H), 3.37 (t, ³J = 4.9 Hz, 2H), 2.27 (td, ⁴J = 2.4 Hz, ³J = 7.0 Hz, 2H), 1.92 (t, ⁴J = 2.3 Hz, 1H), 1.78 (p, ³J = 6.6 Hz, 2H) ppm. ¹³C NMR (63 MHz, CDCl₃) δ = 84.1, 70.8, 70.8, 70.7, 70.7, 70.3, 70.1, 69.7, 68.5, 50.8, 28.6, 15.3, 1.1 ppm. HRMS (ESI-TOF): *m/z* = [M + Na⁺]⁺ Calcd for C₁₃H₂₃N₃O₄Na 308.1581, Found 308.1573.

1-Azido-17-iodo-3,6,9,12-tetraoxaheptadec-16-yne (5)

N-Iodosuccinimide (589 mg, 2.62 mmol, 1.2 eq.) and AgNO₃ (37 mg, 0.22 mmol, 0.1 eq.) were added to a solution of **4** (623 mg, 2.18 mmol) in 40 mL acetone. The reaction mixture was stirred in an inert atmosphere for 4 hours at room temperature in the dark, whereupon a yellow suspension was formed. After concentration of the reaction mixture *in vacuo* the

residue was taken up in CH₂Cl₂ and was washed with an aqueous sodium thiosulfate solution. The solution was extracted with CH₂Cl₂ and the combined organic layers were washed with water. The combined organic layers were dried over sodium sulfate, filtered, and concentrated *in vacuo* to obtain the desired product **5** as yellowish oil in very good yields (778 mg, 87%). To avoid any unwanted click coupling, the reaction and the purification steps were performed at room temperature and the product was stored in the fridge. ¹H NMR (250 MHz, CDCl₃) δ = 3.84 - 3.56 (m, 14H), 3.53 (t, ³J = 6.2 Hz, 2H), 3.39 (t, ³J = 5.0 Hz, 2H), 2.46 (t, ³J = 7.0 Hz, 2H), 1.77 (p, ³J = 6.6 Hz, 2H) ppm. ¹³C NMR (63 MHz, CDCl₃) δ = 94.2, 70.9, 70.8, 70.8, 70.7, 70.4, 70.2, 69.7, 50.9, 28.7, 17.7, -6.9 ppm. HRMS (ESI-TOF): *m/z* = [M + Na⁺]⁺ Calcd for C₁₃H₂₂IN₃O₄Na 434.0547, Found 434.0553.

Scheme S 2: Schematic representation of the cyclisation reaction towards the ion-pair receptors.



The macrocyclization was performed by intramolecular CuAAC cyclization under pseudo-high-dilution conditions using a continuous addition system (adopted from ref. 12).

HB based macrocycle (**6**)

A 250 mL round-bottom flask was charged with 175 mL of an ethanol/water/CH₂Cl₂ (2:1:1) mixture and purged with nitrogen. Successively, copper(II) sulfate (67 mg, 0.42 mmol, 1 eq.) and sodium ascorbate (250 mg, 1.26 mmol, 3 eq.) were added and the mixture was heated to 50 °C and stirred under the exclusion of light under a nitrogen atmosphere. A solution of **4** (120 mg, 0.42 mmol, 1 eq.) in 24 mL of a purged ethanol/water/CH₂Cl₂ (2:1:1) mixture was added dropwise *via* a peristaltic addition pump with a flow of 4 mL/h to the stirred solution at 50 °C. After the complete addition of **4**, the mixture was slowly cooled to room temperature and was stirred under the exclusion of light under a nitrogen atmosphere overnight. Afterwards, 40 drops of *N*-(2-hydroxyethyl)ethylenediaminetriacetic acid (HEEDTA) were added, and the reaction mixture was stirred for 30 min at 50 °C. After cooling to room temperature, the reaction mixture was extracted with water and CH₂Cl₂ and the combined organic phases were concentrated *in vacuo*. The crude product was purified by flash column

chromatography (silica, CH₂Cl₂/methanol (98:2) to CH₂Cl₂/methanol (95:5)) to obtain a colorless oil, which was further recrystallized from diethyl to obtain white crystals of the desired product **7** in good yields (89 mg, 74%). Single crystals were obtained by slow vapor diffusion of *n*-pentane into a concentrated solution of **6** in diethyl ether in the fridge. ¹H NMR (600 MHz, CDCl₃) δ = 7.96 (s, 1H), 4.54 (t, ³J = 4.6 Hz, 2H), 3.82 (t, ³J = 4.6 Hz, 2H), 3.76 - 3.73 (m, 2H), 3.68 - 3.62 (m, 8H), 3.59 - 3.55 (m, 2H), 3.35 (t, ³J = 5.8 Hz, 2H), 2.90 (t, ³J = 6.5 Hz, 2H), 1.93 (p, ³J = 6.6 Hz, 2H) ppm. ¹³C NMR (151 MHz, CDCl₃) δ = 146.8, 124.2, 71.3, 71.2, 71.2, 71.0, 70.6, 70.1, 69.5, 68.5, 49.8, 28.8, 21.3 ppm. HRMS (ESI-TOF): *m/z* = [M + H]⁺ Calcd for C₁₃H₂₄N₃O₄ 286.1761, Found 286.1763.

XB based macrocycle (7)

A 500 mL round-bottom flask was loaded with copper(I)-iodide (278 mg, 1.46 mmol, 1 eq.) and *tris*((1-benzyl-1*H*-1,2,3-triazol-4-yl)methyl)amine (TBTA) (774 mg, 1.46 mmol, 1 eq.) dissolved in 330 mL dry THF. The mixture was heated to 40 °C and stirred for one hour under the exclusion of light under a nitrogen atmosphere. A solution of **5** (600 mg, 1.46 mmol, 1 eq.) in 24 mL of dry THF was added dropwise *via* a peristaltic addition pump with a flow of 4 mL/h to the stirred solution at 40 °C. After the complete addition of **5**, the mixture was stirred at 40 °C under the exclusion of light under a nitrogen atmosphere overnight. Afterwards, 25 mL of a 10% NH₄OH solution were added, and the reaction mixture was stirred for one hour at room temperature. After concentration of the reaction mixture *in vacuo* the residue was taken up in CH₂Cl₂, washed subsequently with water and was again concentrated *in vacuo*. The crude product was purified by a short column chromatography (silica, CH₂Cl₂/diethyl ether (3:7)) to obtain the desired product **7** as a yellowish solid in good yields (450 mg, 75%). Single crystals were obtained by slow vapor diffusion of *n*-pentane into a concentrated solution of **7** in CH₂Cl₂. ¹H NMR (400 MHz, CDCl₃) δ = 4.55 (t, ³J = 4.8 Hz, 2H), 3.94 (t, ³J = 5.0 Hz, 2H), 3.59 - 3.46 (m, 14H), 2.78 (t, ³J = 6.3 Hz, 2H), 2.09 (p, ³J = 6.5 Hz, 2H) ppm. ¹³C NMR (101 MHz, CDCl₃) δ = 150.8, 80.5, 71.7, 71.6, 71.3, 71.1, 70.6, 70.6, 69.9, 69.8, 50.7, 28.2, 22.5 ppm. HRMS (ESI-TOF): *m/z* = [M + Na]⁺ Calcd for C₁₃H₂₂IN₃O₄Na 434.0547, Found 434.0542.

2. NMR spectra:

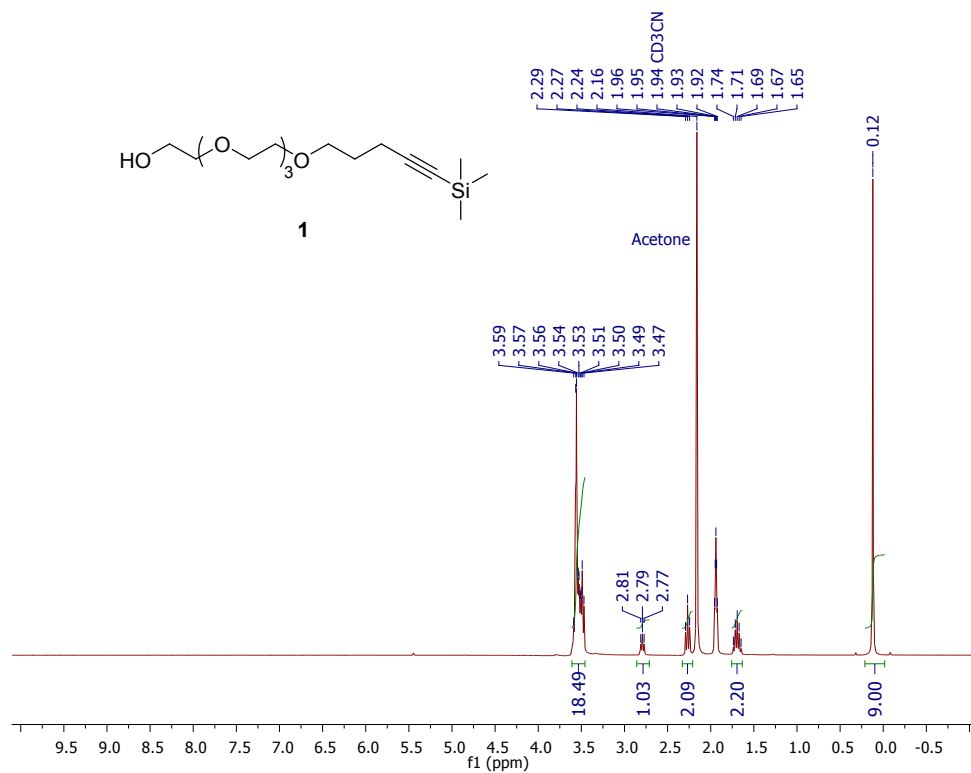


Figure S 1: ¹H NMR (300 MHz, CD₃CN) of **1**.

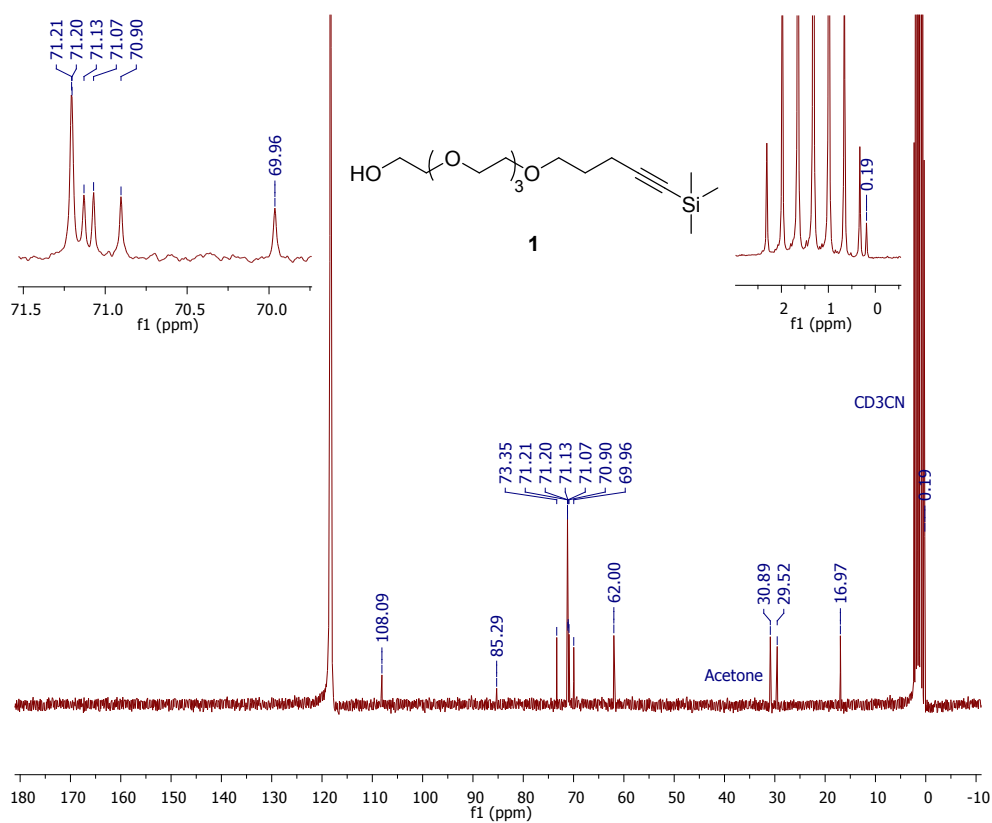


Figure S 2: ¹³C NMR (63 MHz, CD₃CN) of **1**.

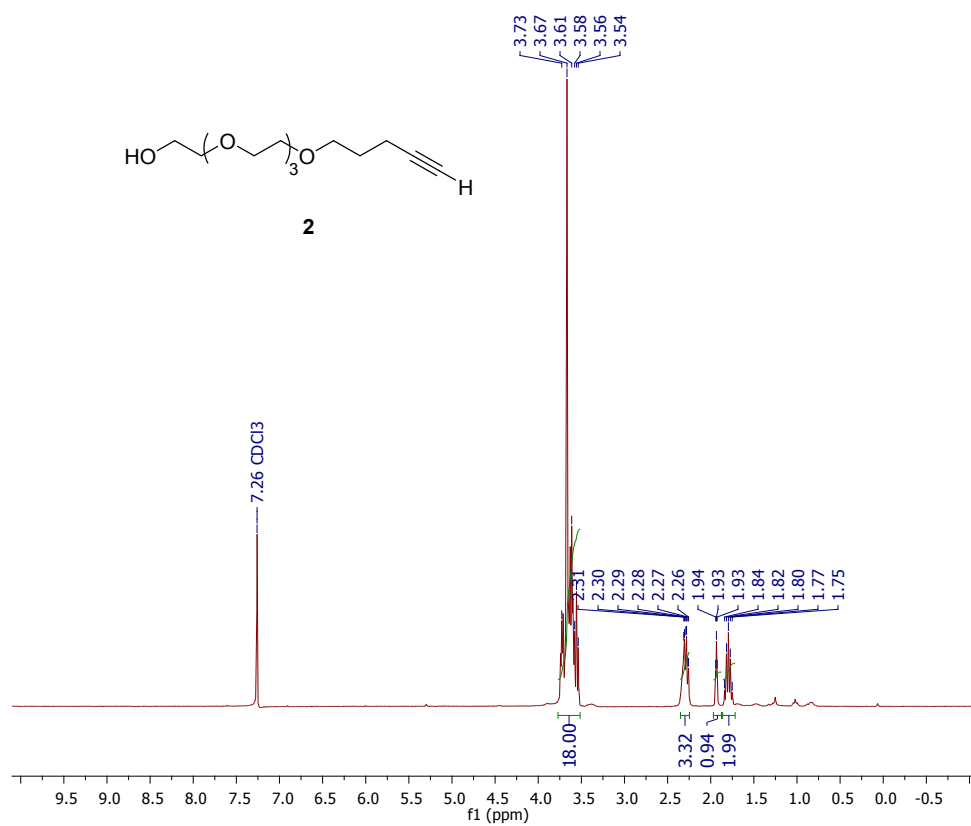


Figure S 3: ¹H NMR (300 MHz, CDCl₃) of **2**.

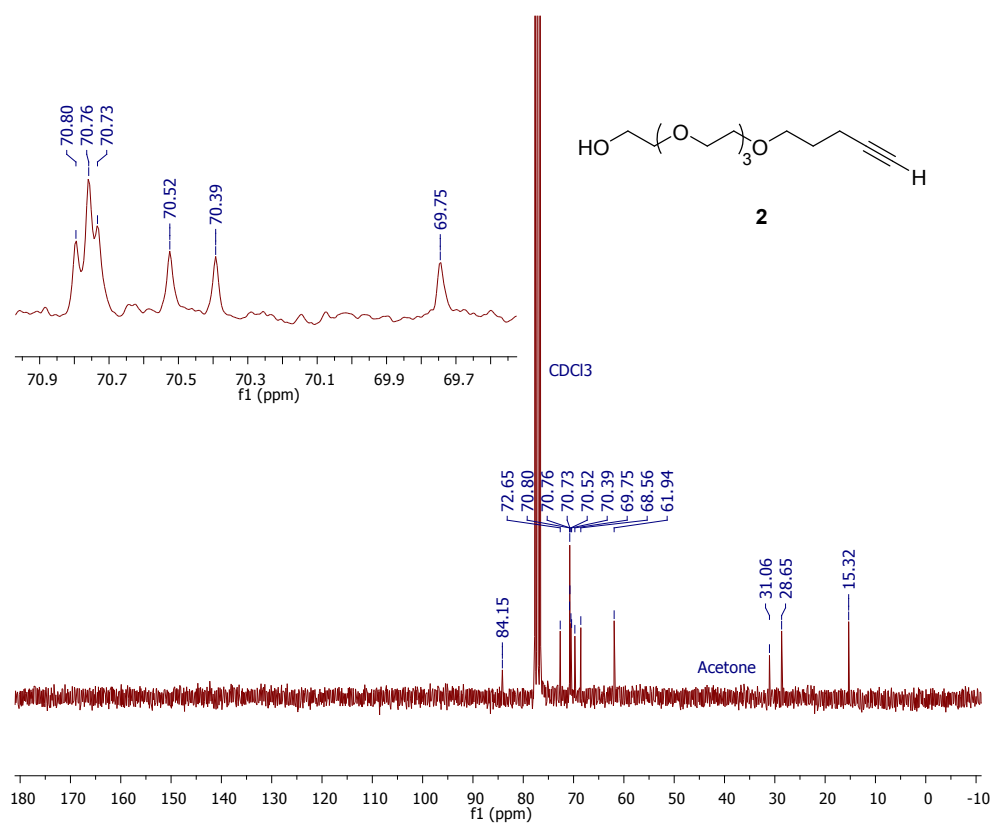


Figure S 4: ¹³C NMR (63 MHz, CDCl₃) of **2**.

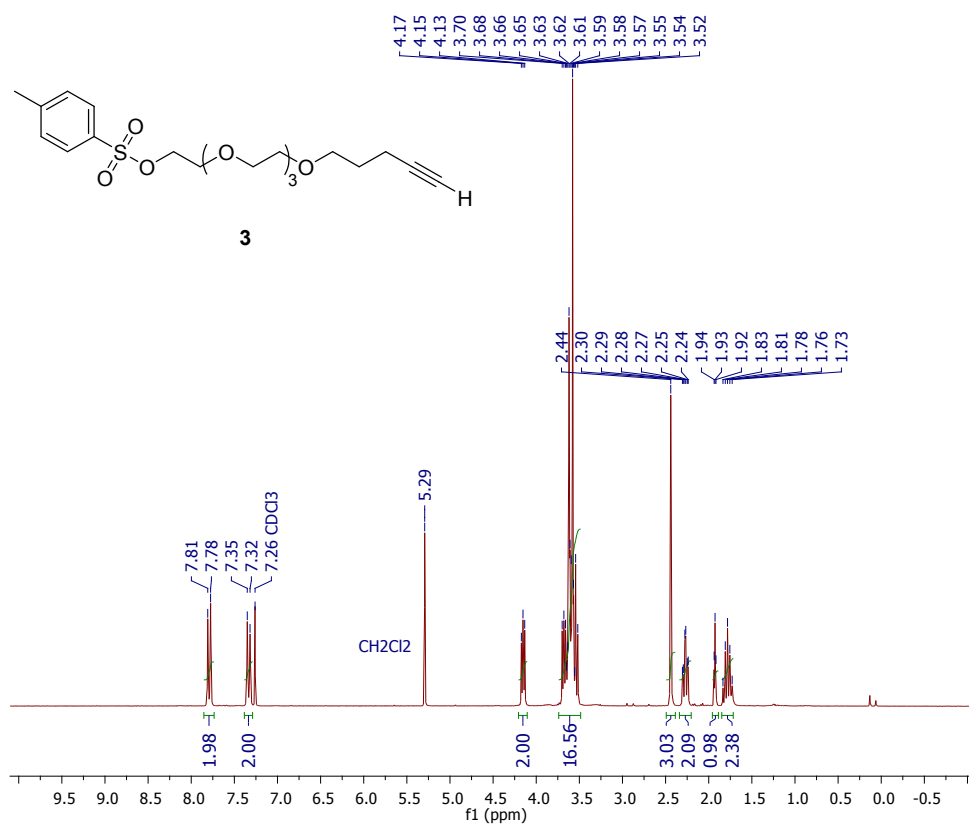


Figure S 5: ^1H NMR (250 MHz, CDCl_3) of 3.

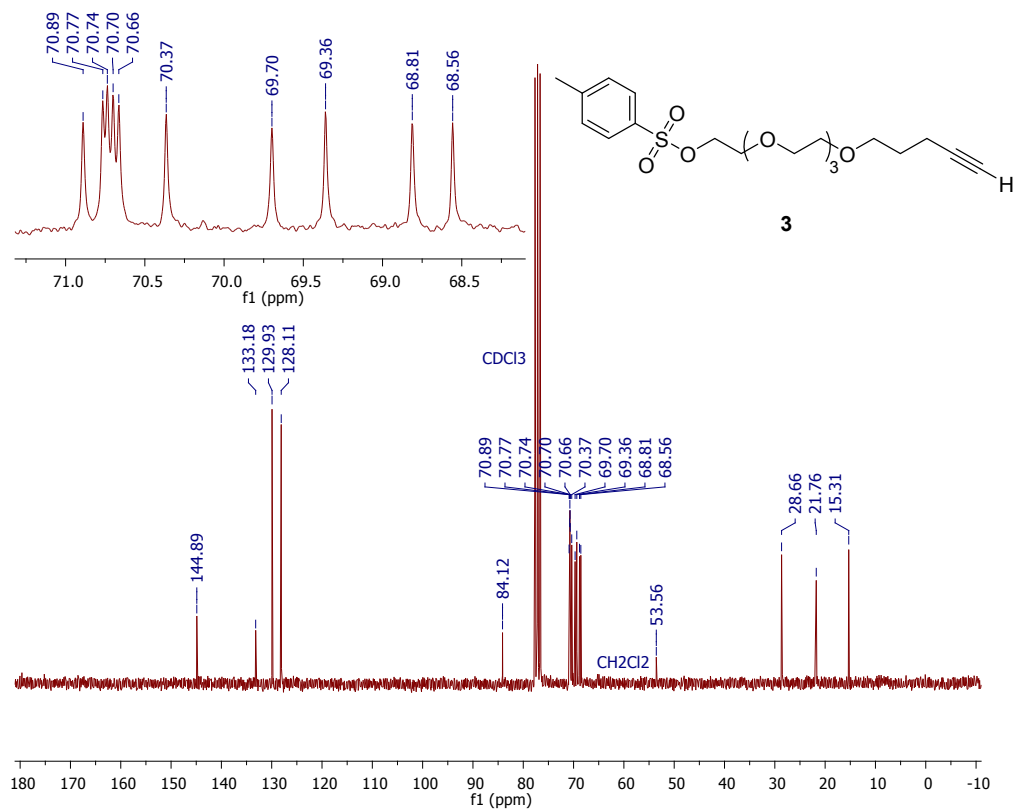


Figure S 6: ^{13}C NMR (63 MHz, CDCl_3) of 3.

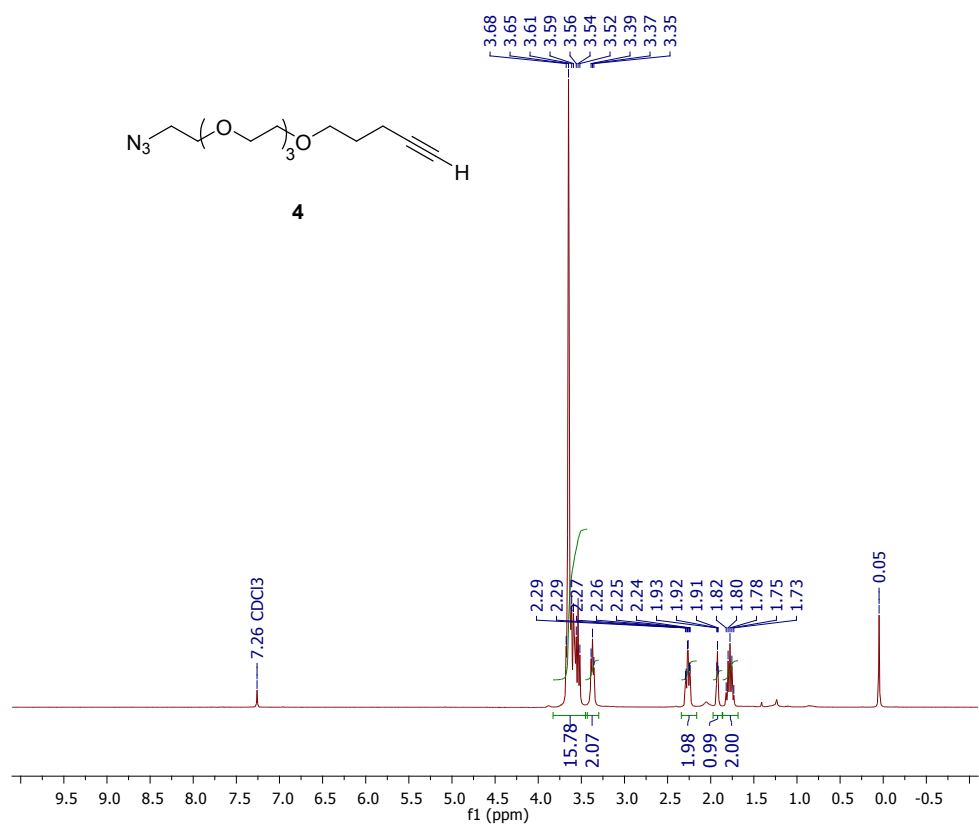


Figure S 7: ¹H NMR (300 MHz, CDCl₃) of 4.

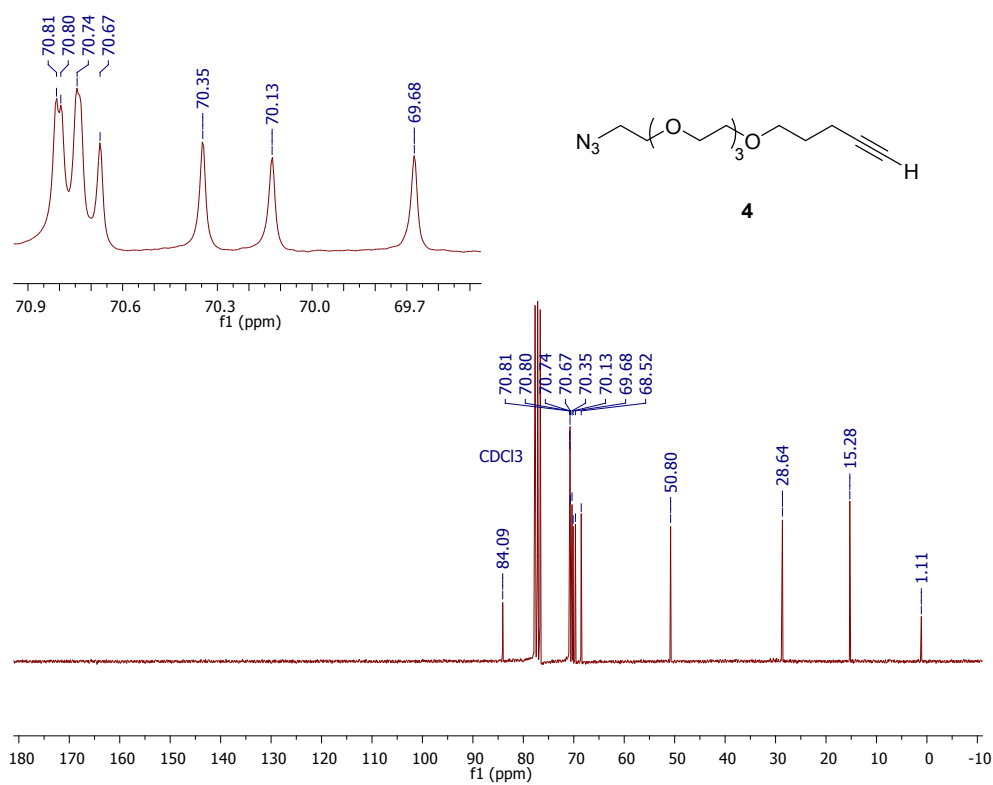


Figure S 8: ¹³C NMR (63 MHz, CDCl₃) of 4.

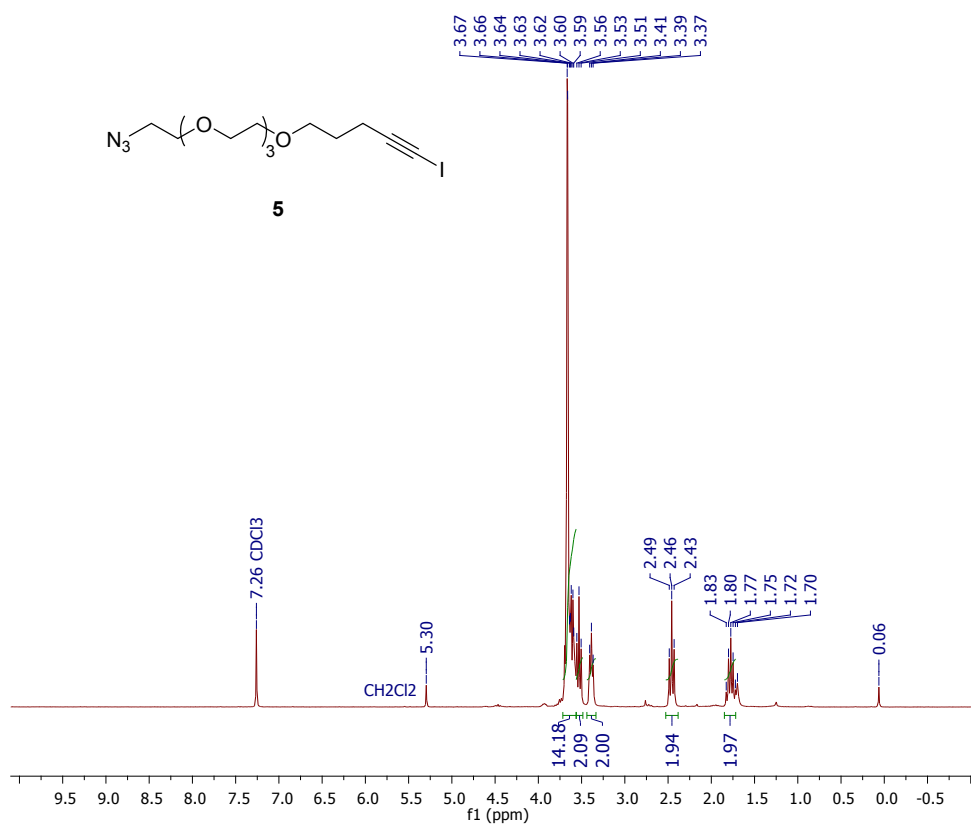


Figure S 9: ¹H NMR (250 MHz, CDCl₃) of **5**.

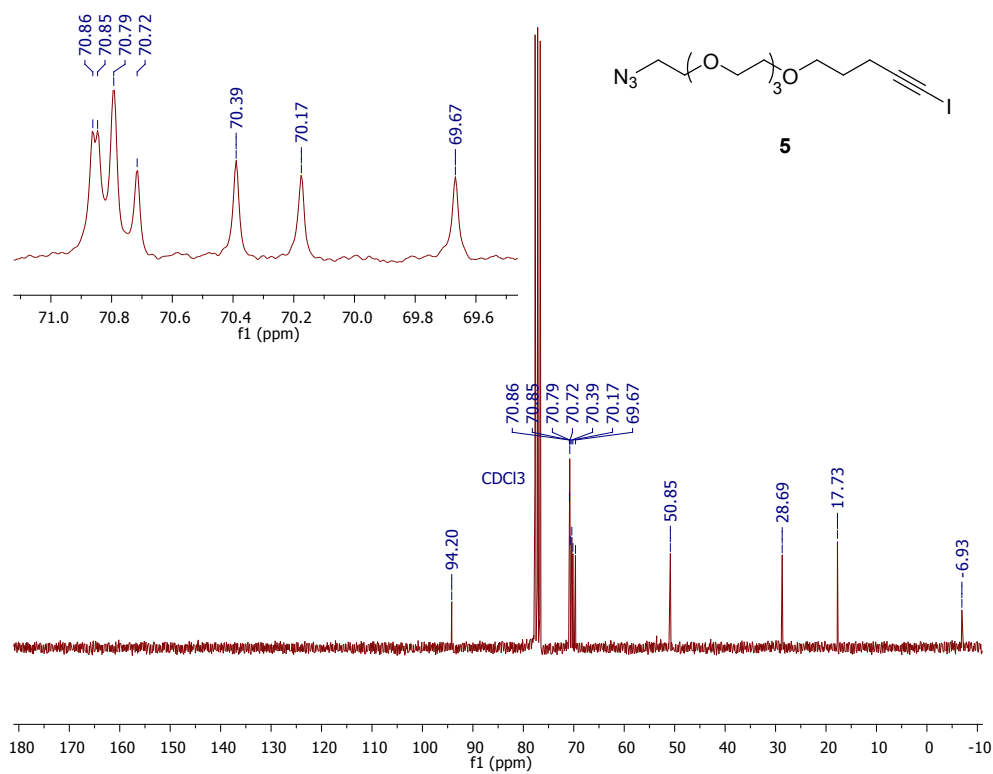


Figure S 10: ¹³C NMR (63 MHz, CDCl₃) of **5**.

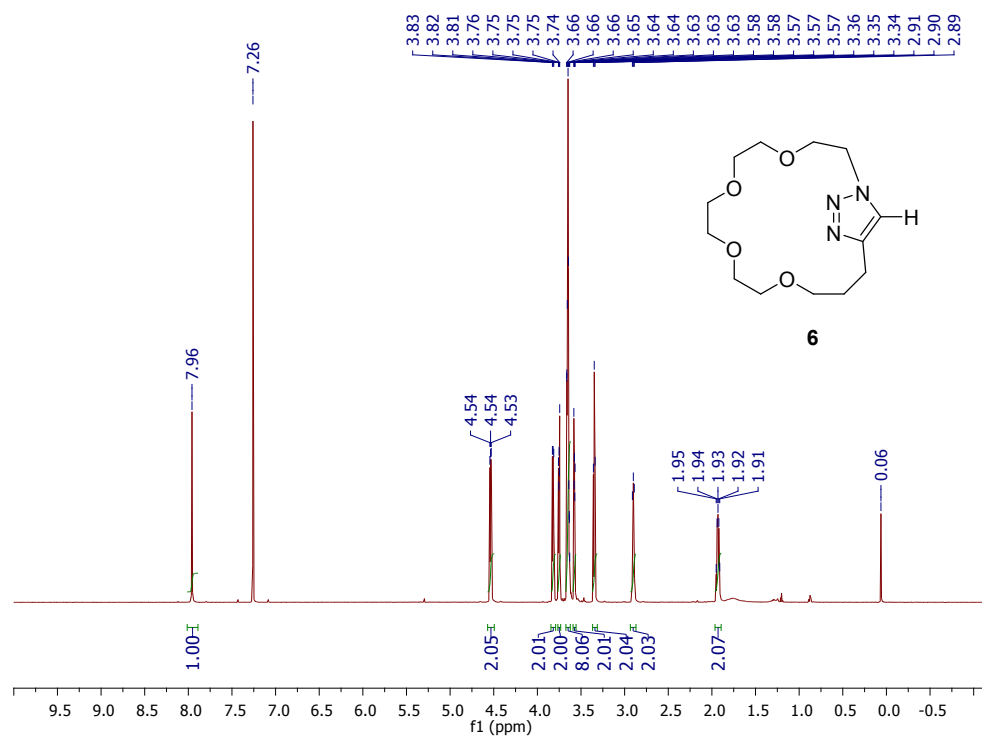


Figure S 11: ^1H NMR (600 MHz, CDCl_3) of 6.

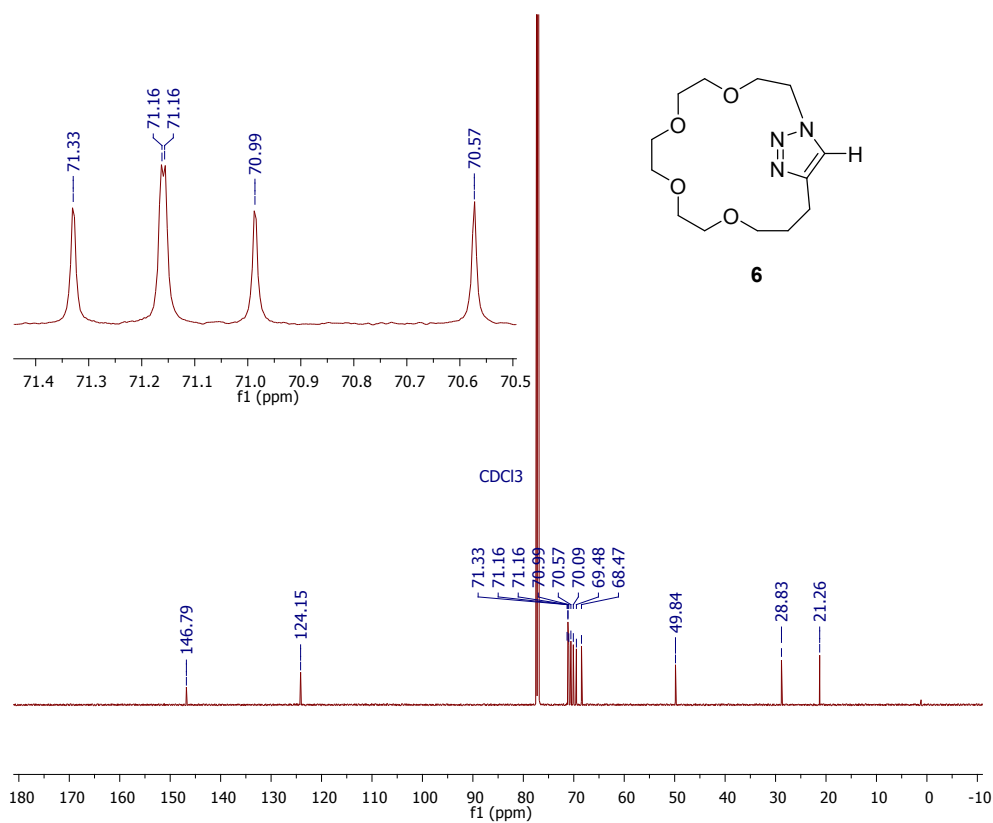


Figure S 12: ^{13}C NMR (151 MHz, CDCl_3) of 6.

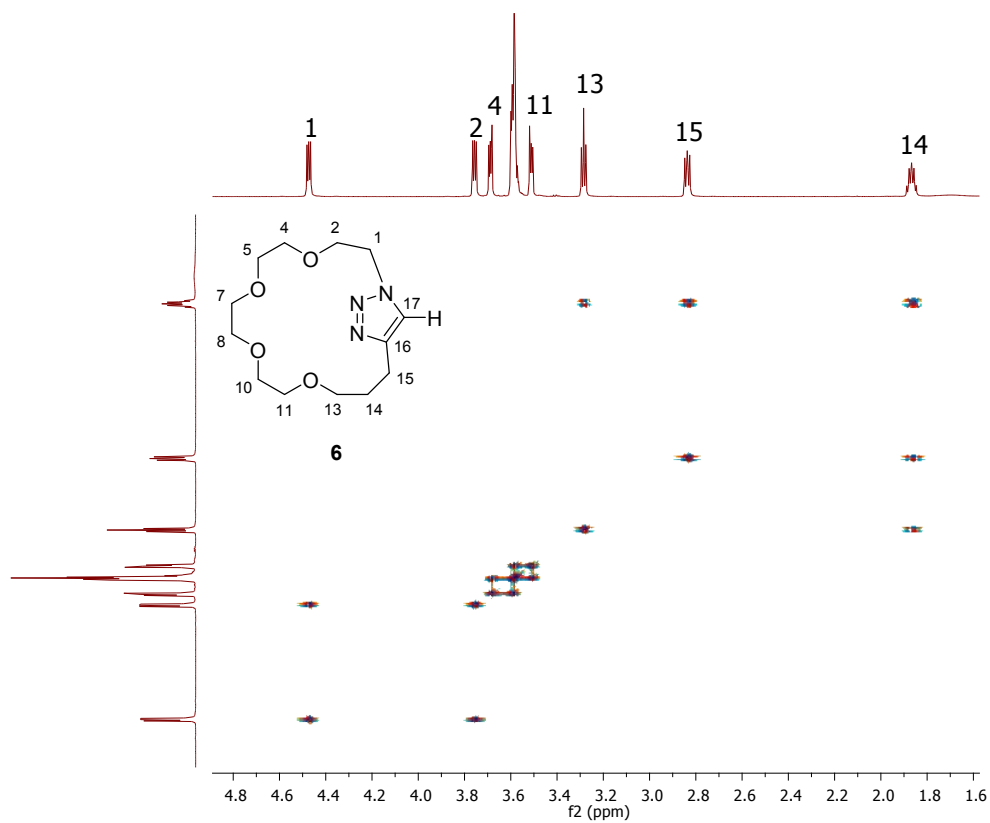


Figure S 13: $^1\text{H}/^1\text{H}$ COSY NMR (600 MHz, CDCl_3) of **6**.

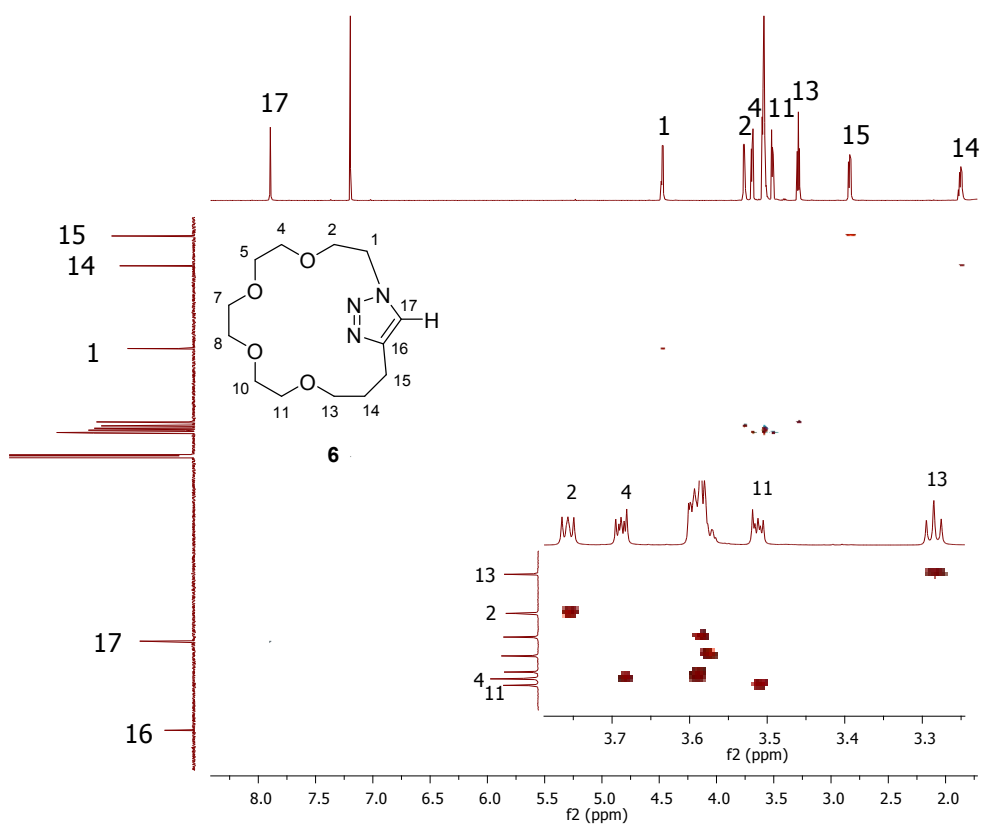


Figure S 14: ^1H , ^{13}C HSQC NMR (600/151 MHz, CDCl_3) of **6**.

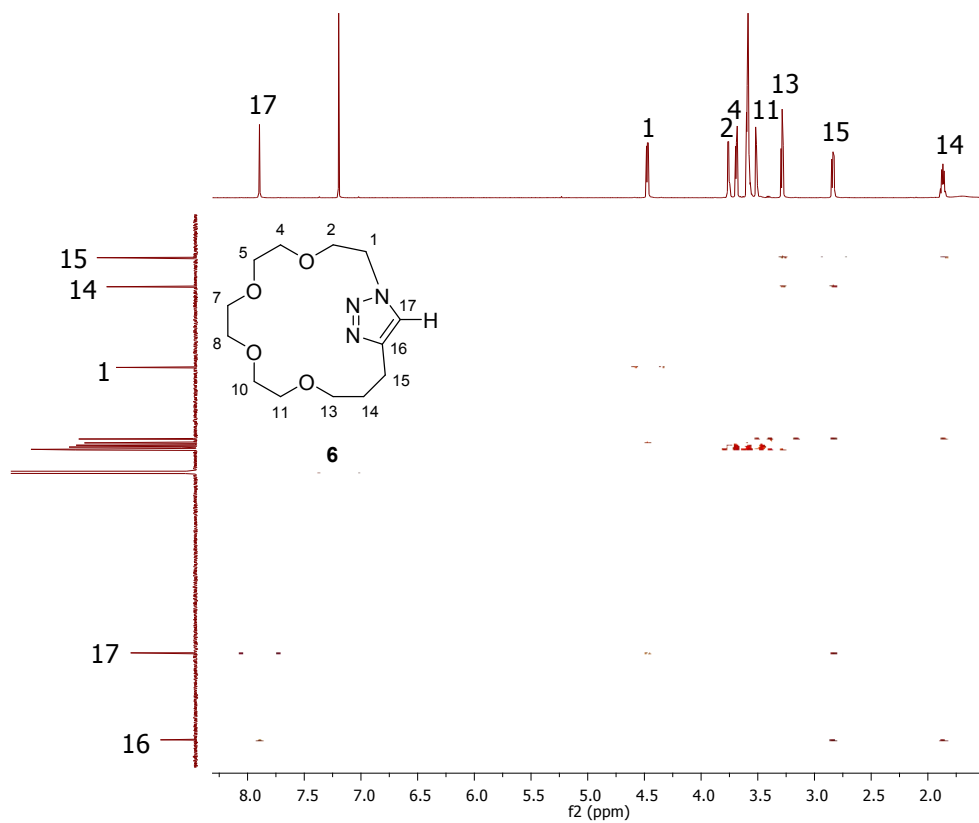


Figure S 15: ^1H , ^{13}C HMBC NMR (600/151 MHz, CDCl_3) of **6**.

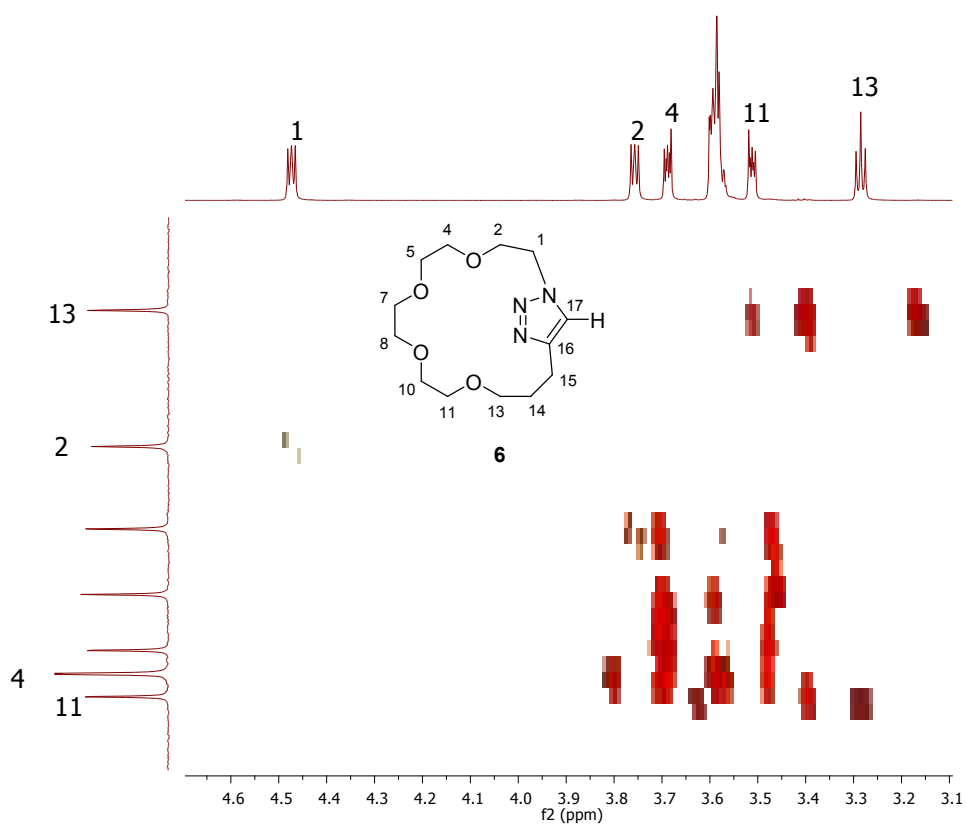
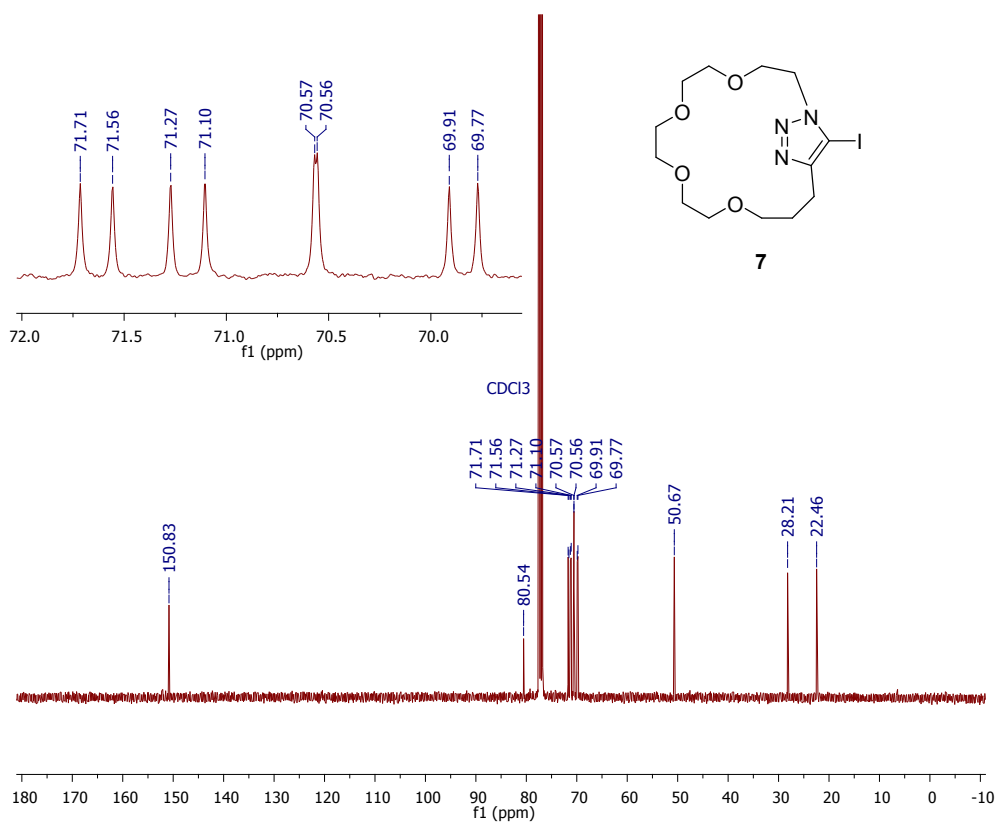
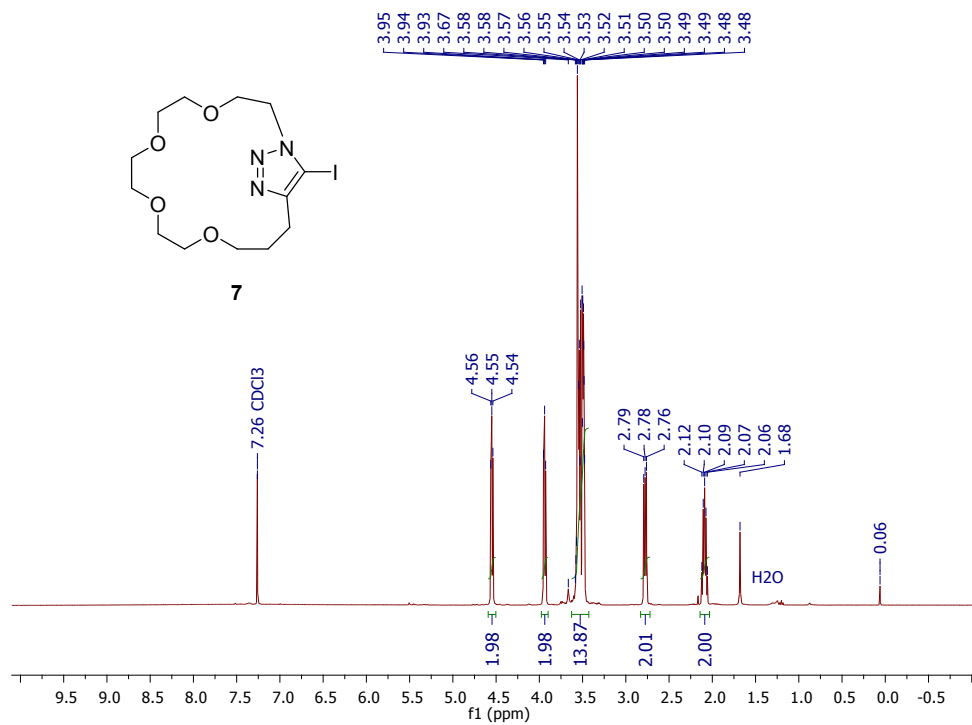


Figure S 16: ^1H , ^{13}C HMBC NMR (600/151 MHz, CDCl_3) of **6**.



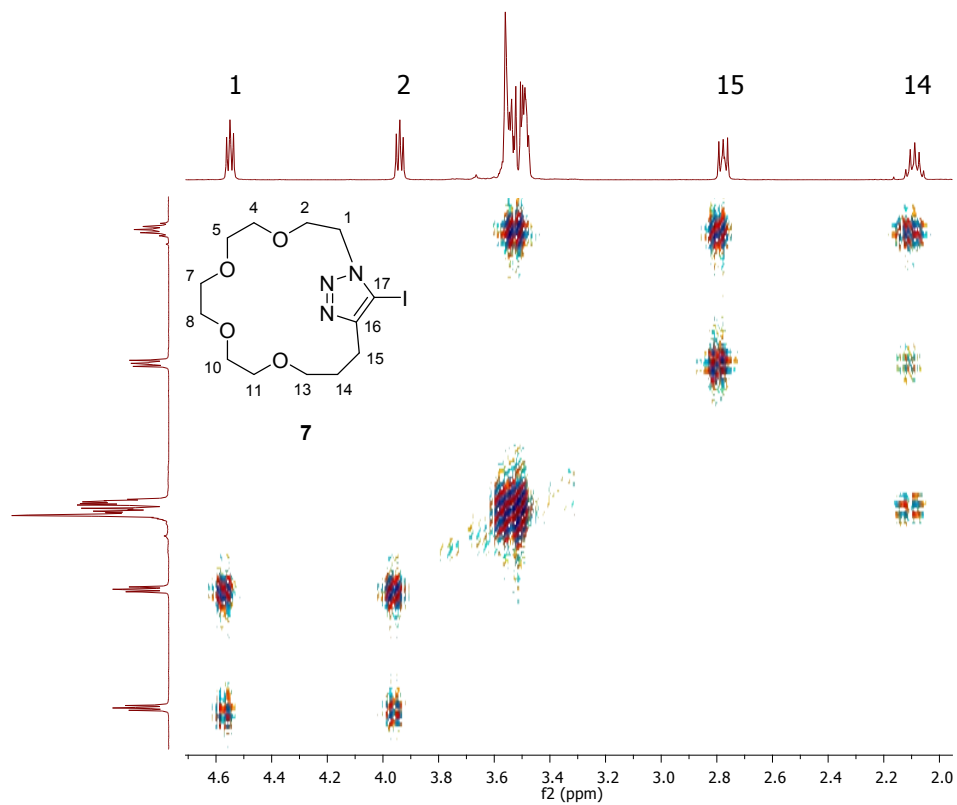


Figure S 19: $^1\text{H}/^1\text{H}$ COSY NMR (400 MHz, CDCl_3) of **7**.

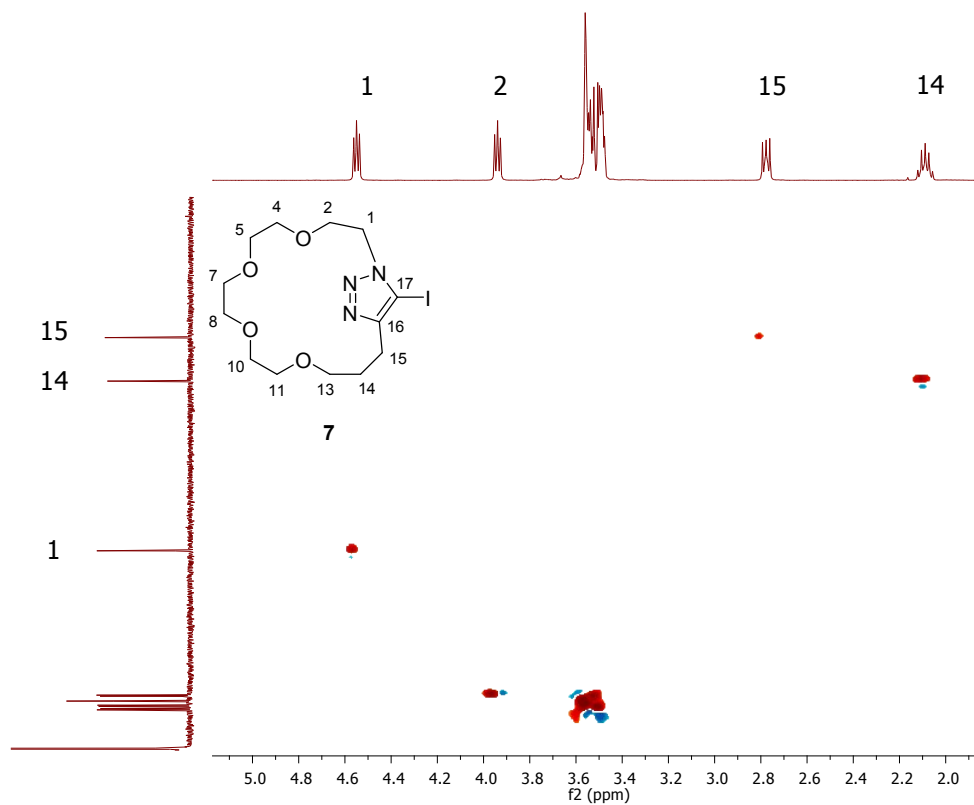


Figure S 20: $^1\text{H}, ^{13}\text{C}$ HSQC NMR (400/101 MHz, CDCl_3) of **7**.

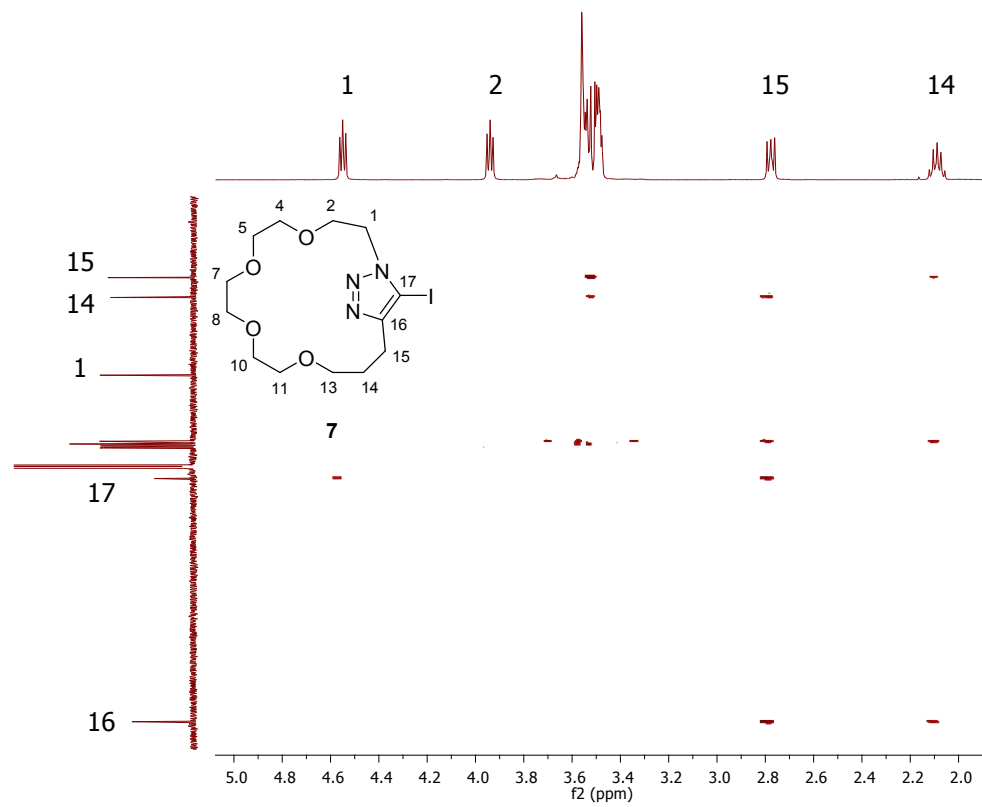


Figure S 21: ^1H , ^{13}C HMBC NMR (400/101 MHz, CDCl_3) of **7**.

3. NMR analysis:

Titration experiment

A stock solution of the studied host was prepared in the listed concentration and corresponding solvent mixture (**Table S 1**). The stock solution of the guest ($[Guest] = 20 \times [Host]$) was prepared by dissolving the appropriate amount of salt in 1 mL stock solution of the host. By the help of this method, there were no changes in the host concentration during the titration as a result of dilution effects. The general titration experiment consists of a sequential addition of the guest stock solution to a 0.5 mL aliquot of the host stock solution directly into the NMR tube. In all cases, a solvent signal was used as an internal standard for calibration (see Figures displaying the chemical shift of the corresponding titration).

Noteworthy, only a 1 mM host solution could be used for the experiments with sodium iodide due to solubility issues of the salt in the corresponding solvent mixture. Consequently, acquisition times of nearly one day and a nitrogen-cooled direct observe NMR probe (“Prodigy BBO”, Bruker BioSpin) providing increased selectivity were required to detect the quaternary ^{13}C signal of the C_{17} atom used for the calculation of the anion binding affinity. Hence, to ensure a consistent solvent mixture and to guarantee comparability between each measuring point, the host as well as guest stock solutions for each data point were prepared immediately before the measurements. Moreover, to proof the consistency of the freshly prepared solvent mixtures, tetraethylsilane ($Si(Et)_4$) was added as an additional internal standard (see Figures displaying the chemical shift of the corresponding ^{13}C NMR titration).

At the end of the titration experiment, the 1H NMR as well as ^{13}C NMR chemical shifts were plotted against the added equivalents of guest to obtain the binding isotherms, which were analyzed by the help of the WinEQNMR2¹³ software to calculate the binding constants. In this context, **Figure S 22** exemplary shows a schematic representation of the $^1H/^{13}C$ NMR chemical shifts of host **7** used for the calculation of the cation or anion binding affinities. Moreover, **Table S 1** shows the detailed experimental setup for each measurement including information about the solvent mixture, the host concentration as well as the NMR technique used for the calculation of the binding constants.

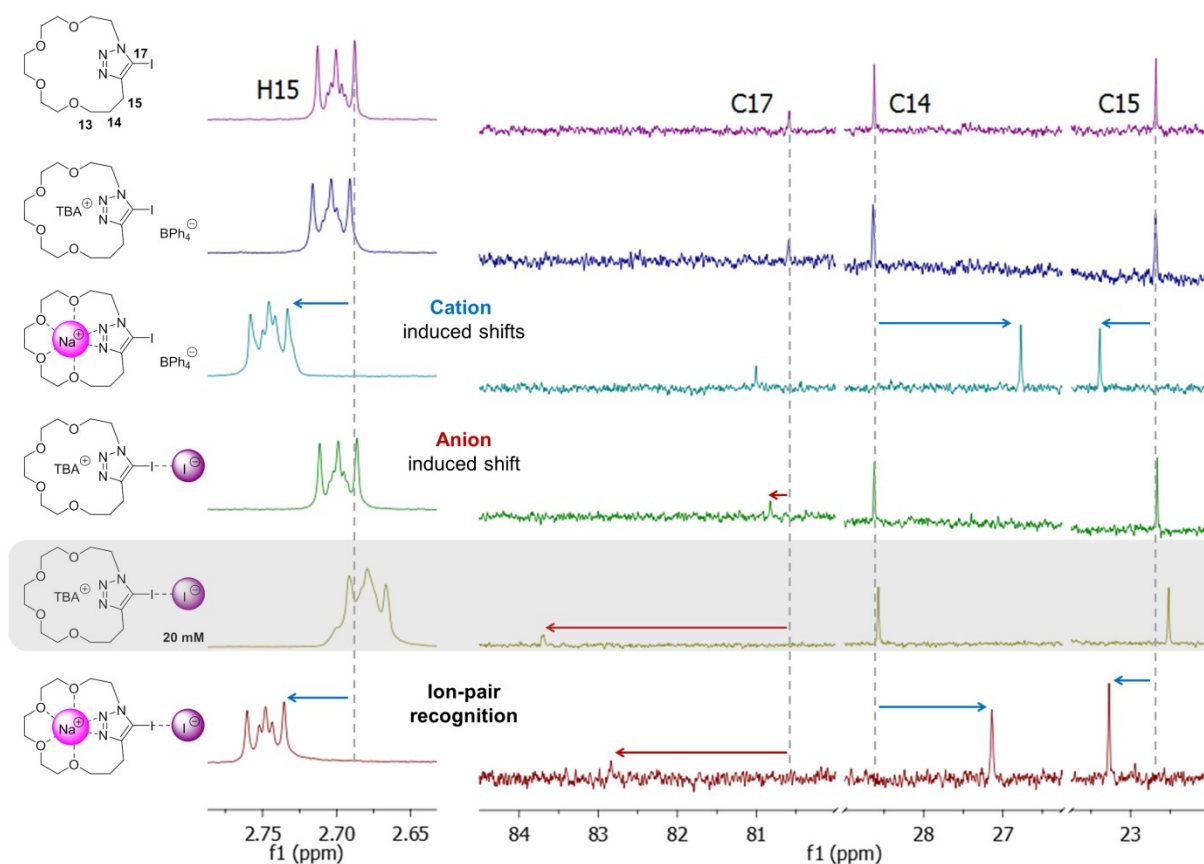
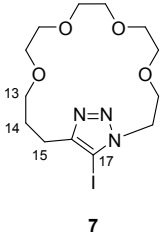
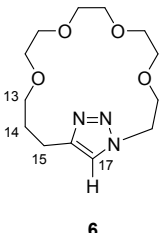


Figure S 22: Schematic representation of the $^1\text{H}/^{13}\text{C}$ NMR (500/126 MHz, $\text{CD}_2\text{Cl}_2:\text{CD}_3\text{CN}$ 3:1) of host **7** [generally 1 mM or 20 mM as depicted] with 8 eq of different guests illustrating the chemical shifts used for the calculation of the cation or anion binding affinities.

Noteworthy, due to a very weak binding affinity of **7** towards iodide caused by: **1)** neutral and thus not charge-assisted triazole moiety; **2)** monodentate interaction; **3)** rather low charge-density/basicity of iodide; **4)** triazole moiety not activated by cation complexation, the anion induced shift for the titration of **7** [1mM] with TBAI was insufficient. Hence, to increase the chemical shift of the C_{17} signal, higher concentrations of **7** [20mM] were used.

Moreover, also the interaction of **7** with NaBPh_4 causes a slight shift of the C_{17} signal. This shift is attributed to an increased interaction with the BPh_4^- counter ion caused by an activation of the XB *via* the cation complexation. In general, the TBA^+ as well as BPh_4^- counter ion is expected to be unparticipated regarding the cation or the anion binding place, which was proven by the unchanged chemical shifts of **7** during the addition of the TBABPh_4 salt (**Figure S 22**).

Table S 1: Experimental setup for NMR titration measurements.

Host	Guest	Solvent (ratio)	NMR	[Host]	K_{Na} [M^{-1}] ($\Delta\delta$ [ppm]) ^a	K_1 [M^{-1}] ($\Delta\delta$ [ppm]) ^a	information
 7	NaBPh ₄	CD ₂ Cl ₂ :CD ₃ CN (4:1)	¹ H	[2mM]	674 ± 6 ^b (0.06)	-	solvent dependence
		CD ₂ Cl ₂ :CD ₃ CN (3:1)	¹ H	[2mM]	434 ± 6 ^b (0.05)	-	
	TBAI	CD ₂ Cl ₂ :CD ₃ CN (3:1)	¹ H	[1mM]	-	N/S	improved measuring conditions
		CD ₂ Cl ₂ :CD ₃ CN (3:1)	¹³ C	[1mM]	-	N/D ^e (0.24)	
		CD ₂ Cl ₂ :CD ₃ CN (3:1)	¹³ C	[20mM]	-	4.7 ± 0.4 ^e (3.41)	
	NaI	CD ₂ Cl ₂ :CD ₃ CN (3:1)	¹ H	[1mM]	394 ± 14 ^b (0.06)	N/S	comparability ¹ H / ¹³ C NMR
CD ₂ Cl ₂ :CD ₃ CN (3:1)		¹³ C	[1mM]	406 ± 60 ^c (1.66)	135 ± 17 ^e (2.77)		
 6	NaBPh ₄	CD ₂ Cl ₂ :CD ₃ CN (3:1)	¹ H	[2mM]	126 ± 6 ^d (0.16)	-	comparison HB vs. XB
	TBAI	CD ₂ Cl ₂ :CD ₃ CN (3:1)	¹³ C	[20mM]	-	N/D ^e (0.16)	
	NaI	CD ₂ Cl ₂ :CD ₃ CN (3:1)	¹ H	[1mM]	155 ± 19 ^d (0.12)	N/S	
		CD ₂ Cl ₂ :CD ₃ CN (3:1)	¹³ C	[1mM]	174 ± 30 ^c (1.00)	N/D ^e (0.55)	

^a chemical shift of the signal used for the calculation of the corresponding association constant; *b* = H₁₅, *c* = C₁₄, *d* = H₁₃, *e* = C₁₇; N/S = no shift; no anion induced shift observable in the ¹H NMR, which is tentatively assigned to the large distance between the anion binding place and the adjacent hydrogen atoms; N/D = not determined; a reliable quantification of the association constant was not possible due to the insufficient chemical shifts during the NMR titration.

Comparing the cation binding affinities of macrocycle **7** in different solvent mixtures (CD₂Cl₂:CD₃CN 4:1 vs. 3:1), a decreased K_{Na} value with increasing amount of the more polar / competitive CD₃CN was observed. Nevertheless, the CD₂Cl₂:CD₃CN 3:1 mixture had to be used for all the following titrations to provide sufficient solubility for sodium iodide.

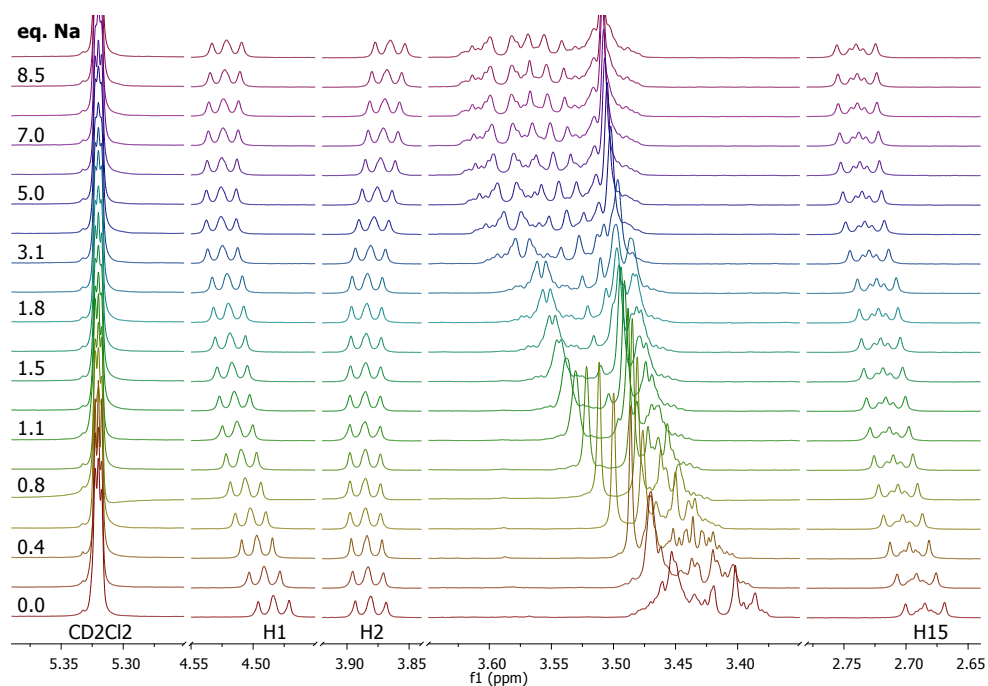


Figure S 23: ^1H NMR chemical shifts of **7** (2 mM stock solution) and NaBPh_4 (40 mM stock solution) in $\text{CD}_2\text{Cl}_2\text{:CD}_3\text{CN}$ (4:1).

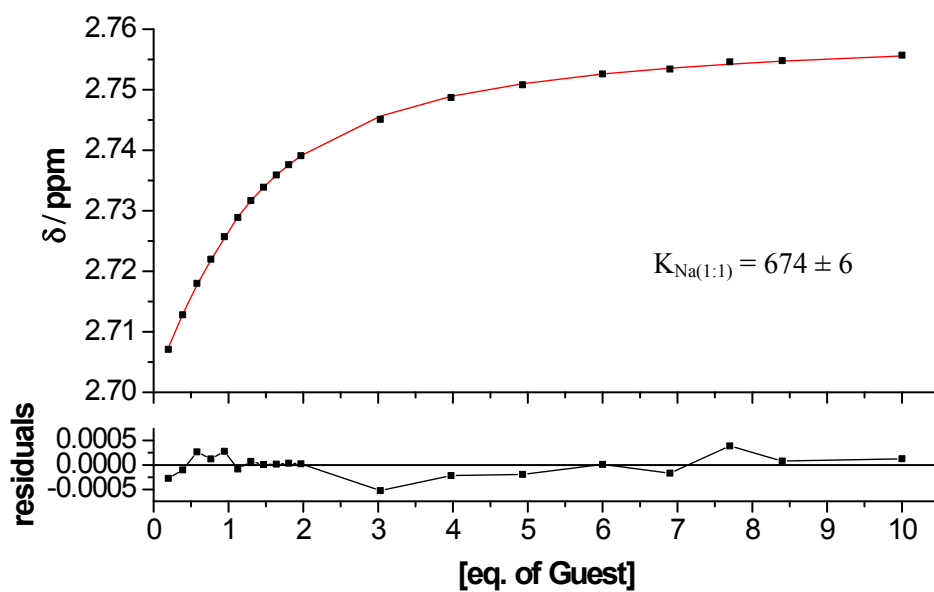


Figure S 24: Analysis of the binding isotherm (H_{15}) of **7** (2 mM stock solution) and NaBPh_4 (40 mM stock solution) in $\text{CD}_2\text{Cl}_2\text{:CD}_3\text{CN}$ (4:1) assuming a 1:1 (Host:Guest) binding model.

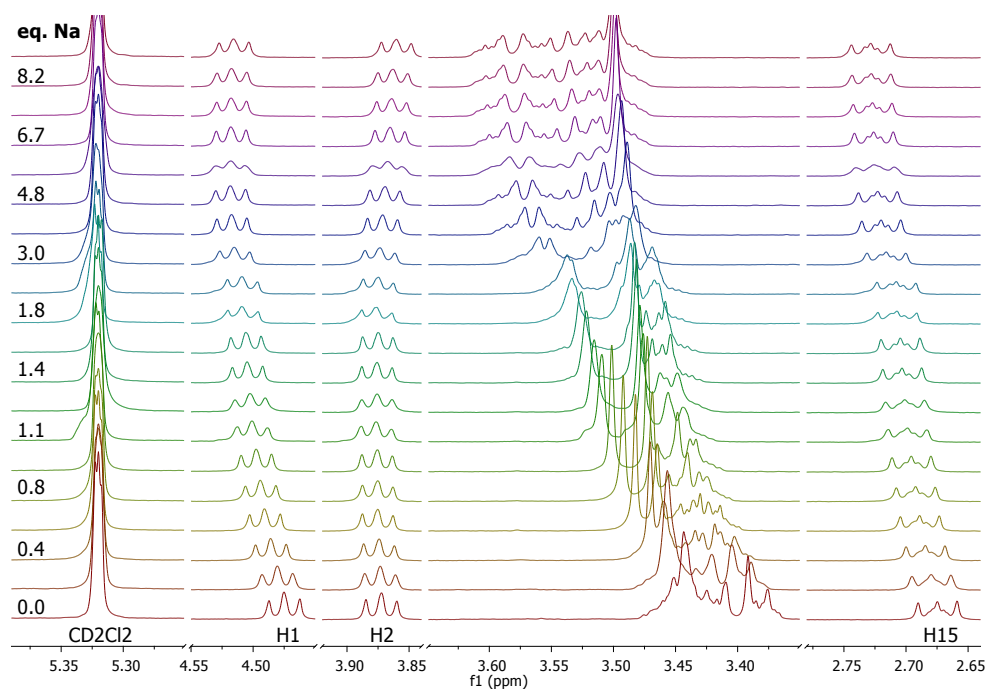


Figure S 25: ¹H NMR chemical shifts of **7** (2 mM stock solution) and NaBPh₄ (40 mM stock solution) in CD₂Cl₂:CD₃CN (3:1).

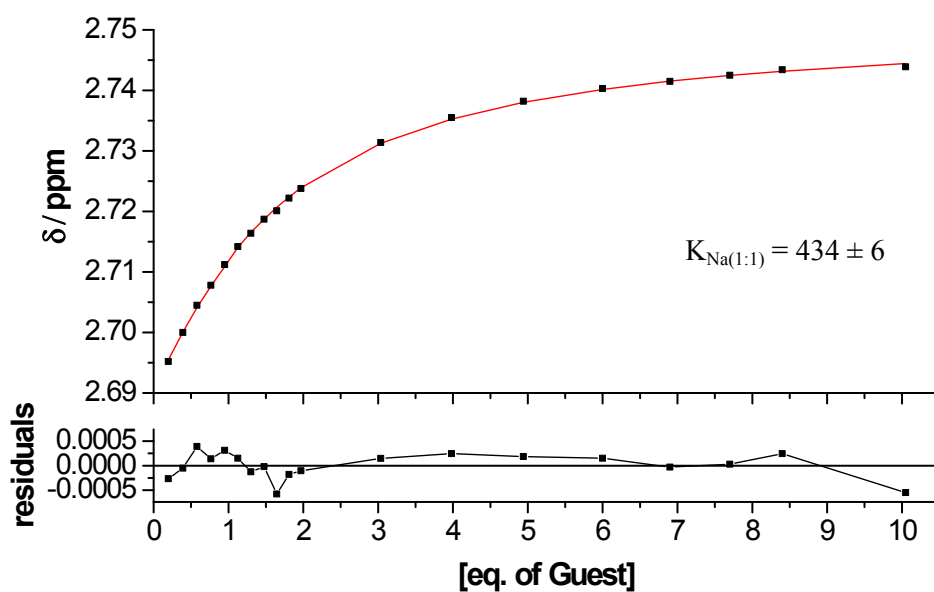


Figure S 26: Analysis of the binding isotherm (H₁₅) of **7** (2 mM stock solution) and NaBPh₄ (40 mM stock solution) in CD₂Cl₂:CD₃CN (3:1) assuming a 1:1 (Host:Guest) binding model.

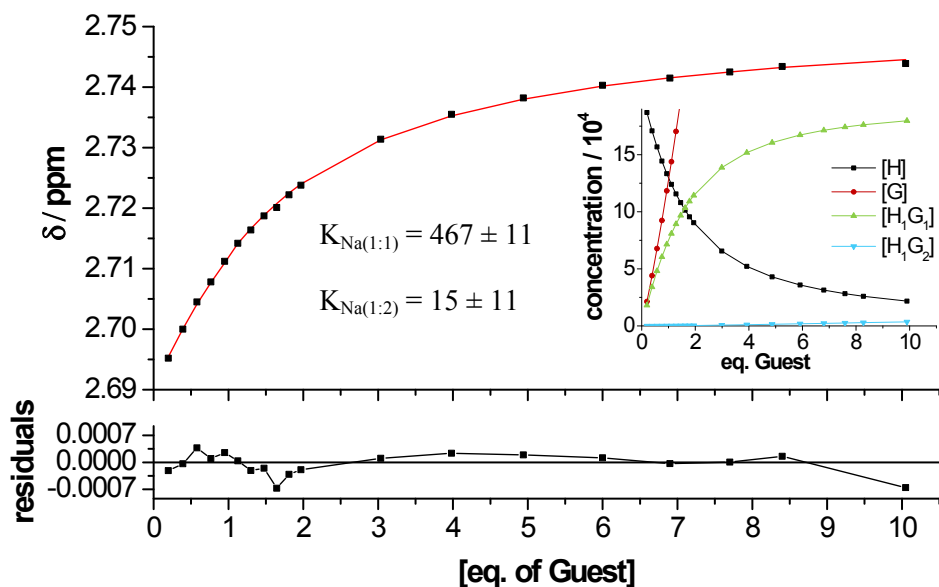


Figure S 27: Analysis of the binding isotherm (H_{15}) of **7** (2 mM stock solution) and NaBPh_4 (40 mM stock solution) in $\text{CD}_2\text{Cl}_2:\text{CD}_3\text{CN}$ (3:1) assuming a 1:2 (Host:Guest) binding model and (inset) speciation curves for all of the involved species (H = host, G = guest).

The solid state analysis also indicated a possible formation of a 1:2 complex with respect to the cation binding place (*vide infra*). Consequently, to exemplarily check the possible contribution of this 1:2 complex also in solution, we assumed a 1:2 binding model to fit the binding isotherm (**Figure S 27**). However, a comparable cation binding affinity for the formation of the 1:1 complex was calculated ($K_{\text{Na}(1:1)} = 434 \pm 6$ assuming a 1:1 binding model vs. $K_{\text{Na}(1:1)} = 467 \pm 11$ assuming a 1:2 binding model) followed by the subsequent formation into a negligible 1:2 complex ($K_{\text{Na}(1:2)} = 15 \pm 11$). Moreover, this predominant formation of the 1:1 complex was also underlined by a Job plot analysis (**Figure S 28**). Consequently, the 1:1 binding model was applied for the analysis of all the binding isotherms, since it should describe the complexation in solution most properly.

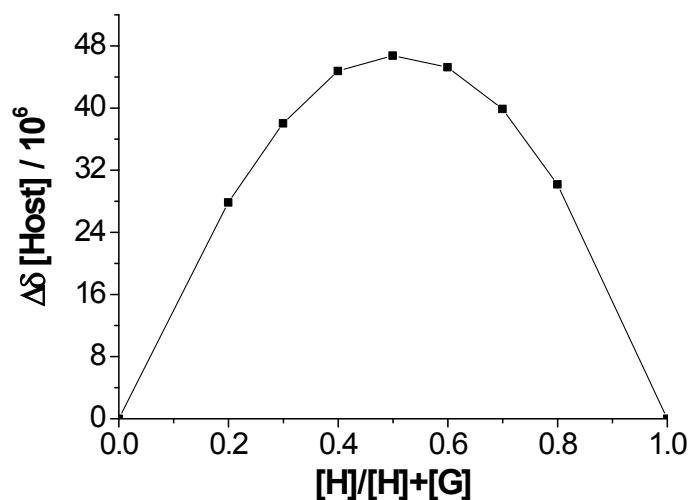


Figure S 28: Job plot analysis (H_{15}) of **7** (4 mM stock solution) and NaBPh_4 in $\text{CD}_2\text{Cl}_2:\text{CD}_3\text{CN}$ (3:1).

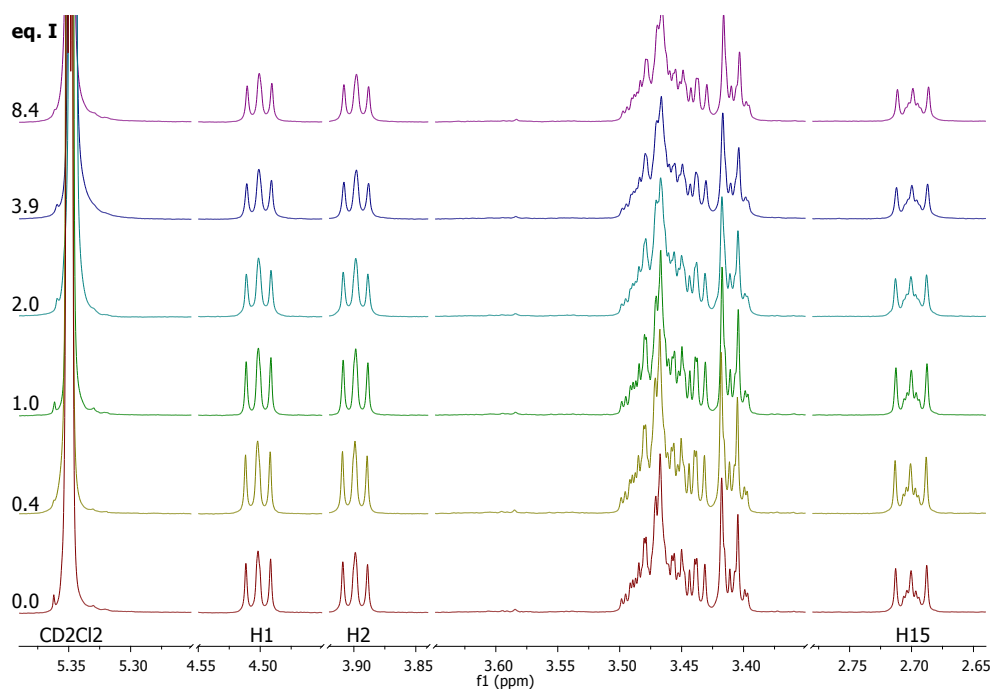


Figure S 29: ^1H NMR chemical shifts of **7** (1 mM stock solution) and Bu_4NI (20 mM stock solution) in $\text{CD}_2\text{Cl}_2\text{:CD}_3\text{CN}$ (3:1).

Figure S 29 clearly demonstrates that there is no anion induced chemical shift observable in the ^1H NMR, which is tentatively assigned to the large distance between the XB based anion binding place and the adjacent hydrogen atoms.

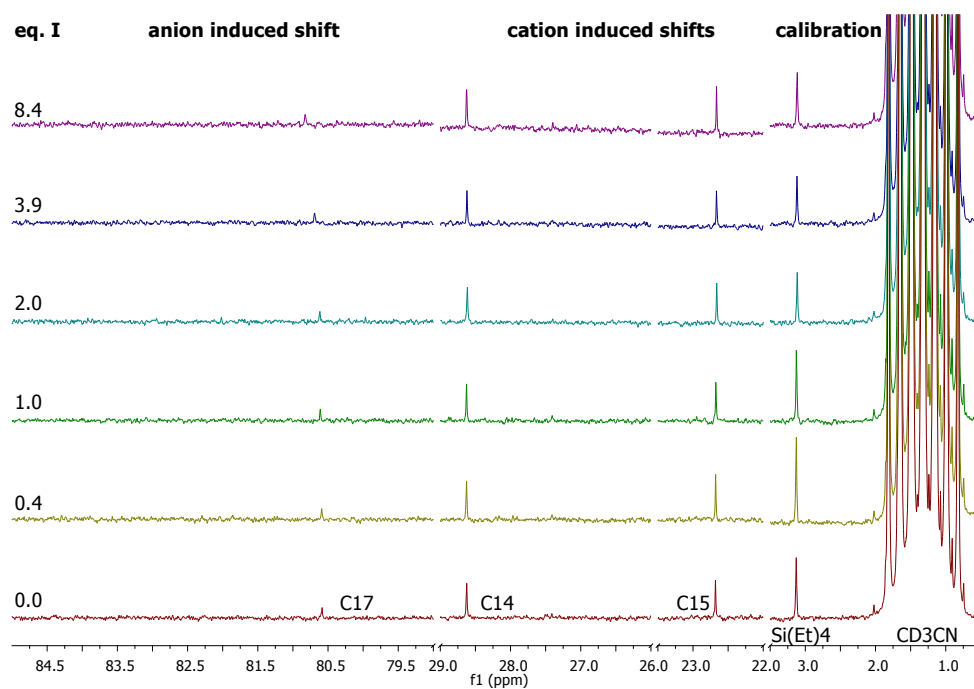


Figure S 30: ^{13}C NMR chemical shifts of **7** (1 mM stock solution) and Bu_4NI (20 mM stock solution) in $\text{CD}_2\text{Cl}_2\text{:CD}_3\text{CN}$ (3:1).

Consequently, the C₁₇ atom which is directly connected to the XB donor atom had to be used for the quantification of the anion binding affinity. Here, a downfield shift of the C₁₇ signal (0.24 ppm for [Host] = 1 mM) was clearly visible; however, this chemical shift was still insufficient for a reliable quantification of the association constant (see **Figure S 30**). Finally, by increasing the host concentration to 20 mM, the chemical shift of the C₁₇ atom could be raised to 3.41 ppm which allowed a reliable quantification. Noteworthy, the chemical shift of C₁₄, used for the calculation of the cation binding affinity, showed no significant shift (C₁₄ = 0.06 ppm for [Host] = 20 mM) verifying the non-coordinating behavior of the tetra-*n*-butylammonium counter ion (see **Figure S 31**).

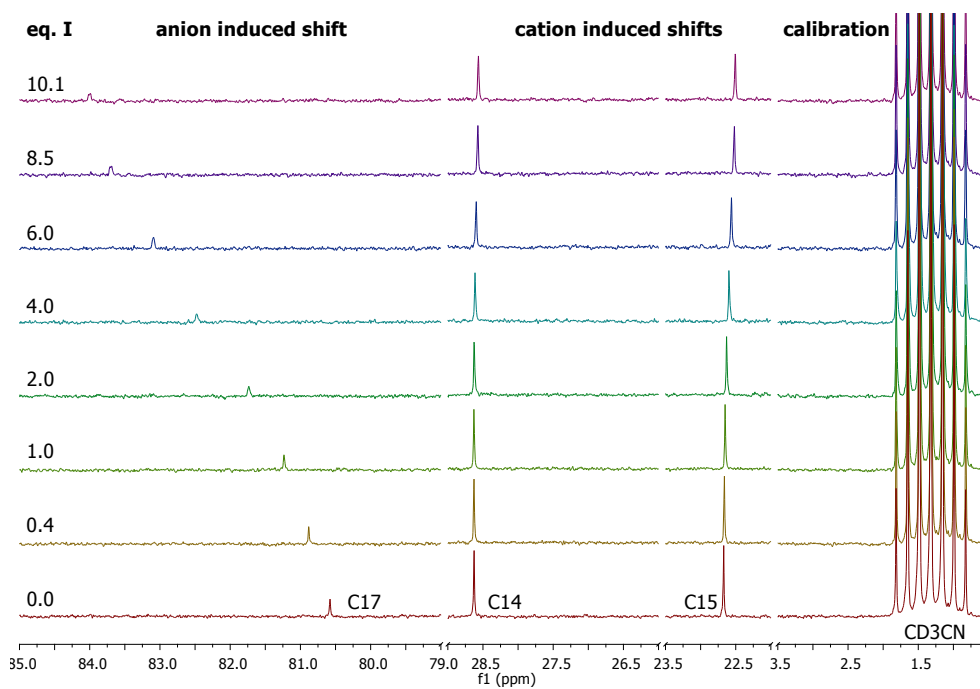


Figure S 31: ^{13}C NMR chemical shifts of 7 (20 mM stock solution) and Bu_4NI (400 mM stock solution) in $\text{CD}_2\text{Cl}_2:\text{CD}_3\text{CN}$ (3:1).

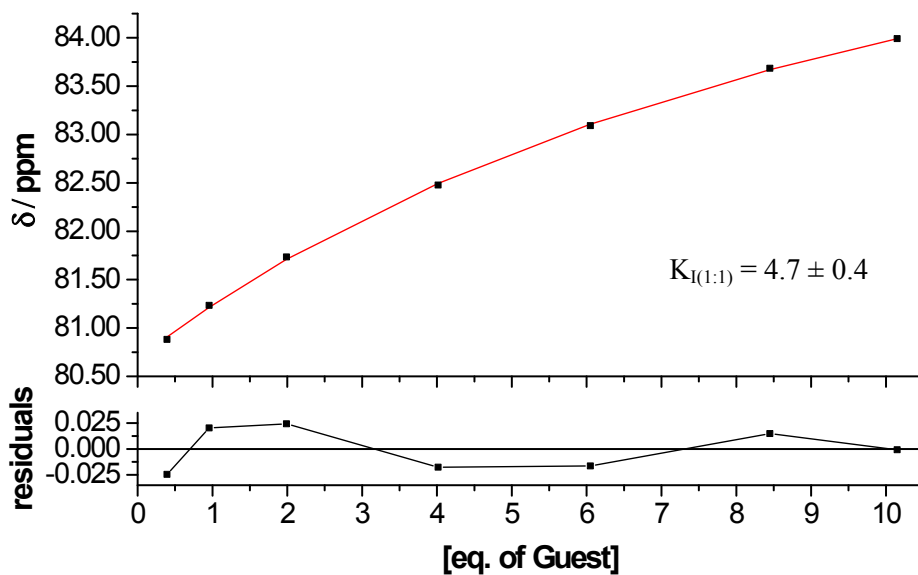


Figure S 32: Analysis of the binding isotherm (C_{17}) of 7 (20 mM stock solution) and Bu_4NI (400 mM stock solution) in $\text{CD}_2\text{Cl}_2:\text{CD}_3\text{CN}$ (3:1) assuming a 1:1 (Host:Guest) binding model.

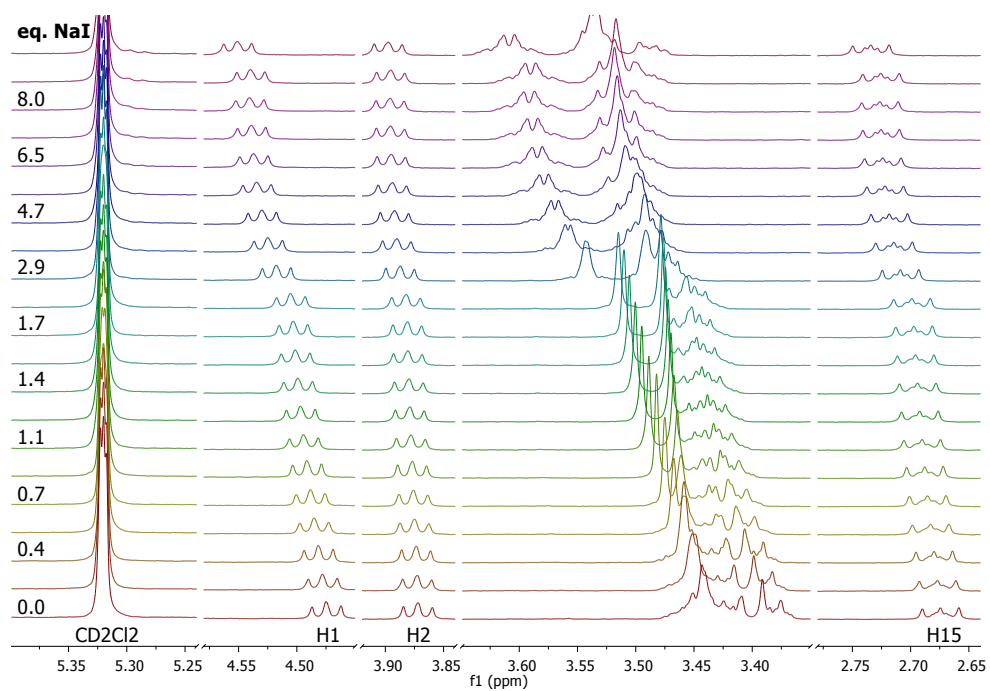


Figure S 33: ¹H NMR chemical shifts of **7** (1 mM stock solution) and NaI (20 mM stock solution) in CD₂Cl₂:CD₃CN (3:1).

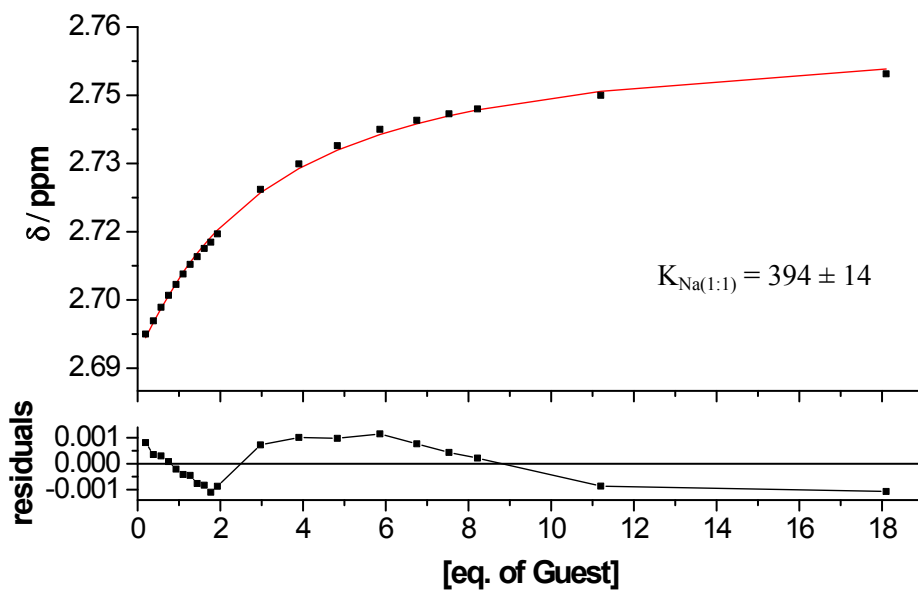


Figure S 34: Analysis of the binding isotherm (H₁₅) of **7** (1 mM stock solution) and NaI (20 mM stock solution) in CD₂Cl₂:CD₃CN (3:1) assuming a 1:1 (Host:Guest) binding model.

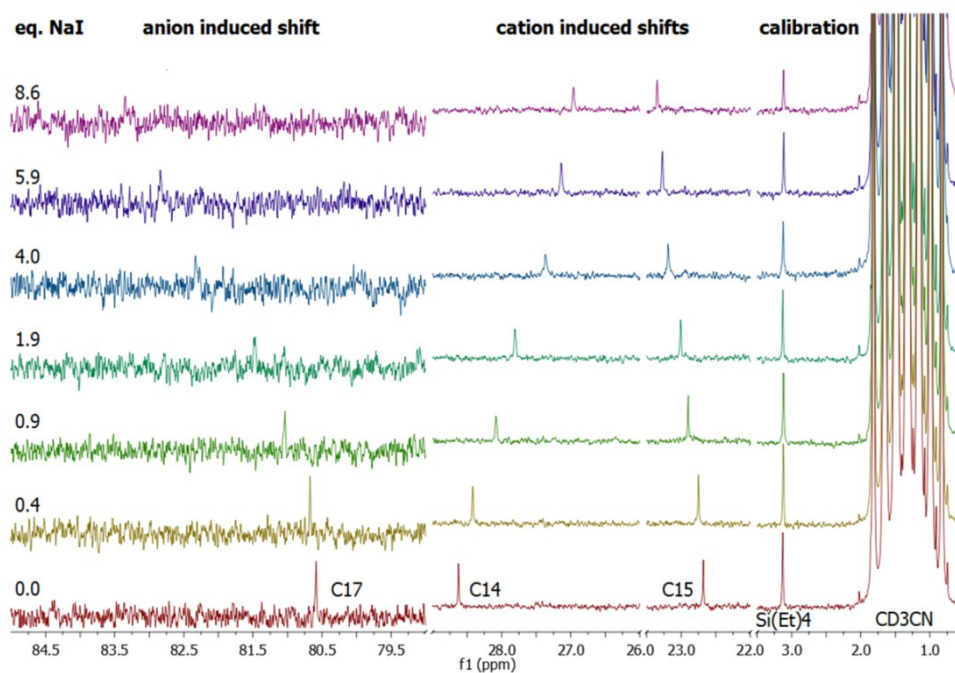


Figure S 35: ^{13}C NMR chemical shifts of **7** (1 mM stock solution) and NaI (20 mM stock solution) in $\text{CD}_2\text{Cl}_2\text{:CD}_3\text{CN}$ (3:1).

Unfortunately, higher concentrations as well as higher equivalents of the added sodium iodide were not possible due to solubility issues. The extensive line broadening observed for the quaternary carbon at higher concentration of NaI also hampered the analysis and is most likely attributed to an unfavorable exchange regime in terms of the NMR time scale.

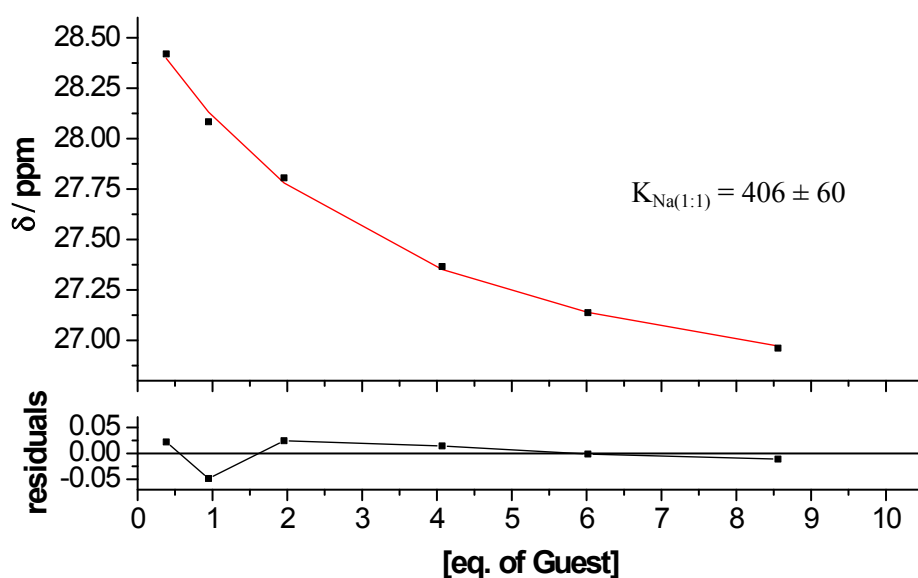


Figure S 36: Analysis of the binding isotherm (C_{14}) of **7** (1 mM stock solution) and NaI (20 mM stock solution) in $CD_2Cl_2:CD_3CN$ (3:1) assuming a 1:1 (Host:Guest) binding model.

Despite fewer data points for the fitting process (accounted by the very long acquisition time of nearly one day for one data point), the cation binding affinities calculated by ^{13}C NMR ($K_{Na} = 406 \pm 60 M^{-1}$) show a very good coincidence with the one calculated by 1H NMR ($K_{Na} = 394 \pm 14 M^{-1}$). This fact further underlines the good comparability between 1H and ^{13}C NMR titration experiments even by changing the atom position used for the calculation (H_{15} vs. C_{14}).

Moreover, the cation binding affinity calculated by the titration of $7 \times NaBPh_4$ ($K_{Na} = 434 \pm 6 M^{-1}$) revealed nearly the same result as the titration of $7 \times NaI$ ($K_{Na} = 394 \pm 14 M^{-1}$) indicating the independence of the cation binding place from the anion.

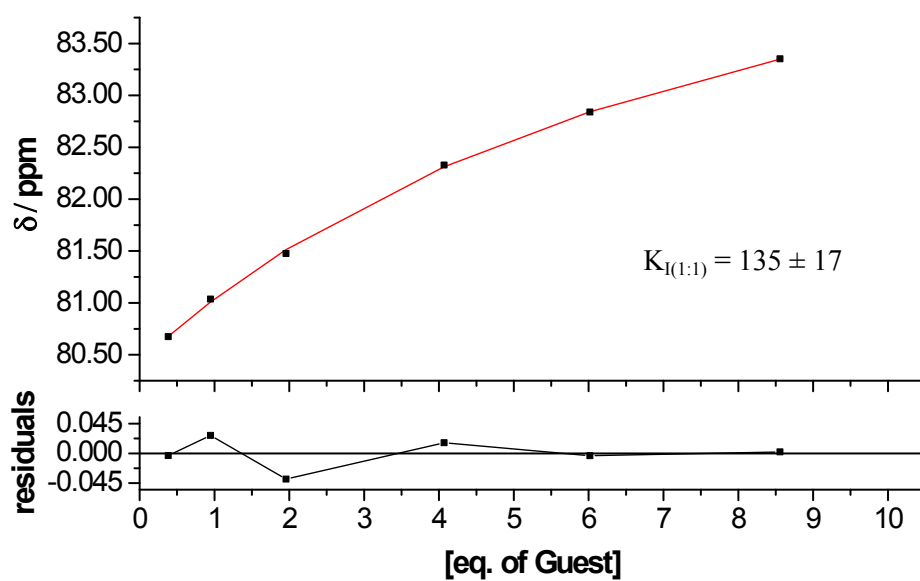


Figure S 37: Analysis of the binding isotherm (C_{17}) of 7 (1 mM stock solution) and NaI (20 mM stock solution) in CD₂Cl₂:CD₃CN (3:1) assuming a 1:1 (Host:Guest) binding model.

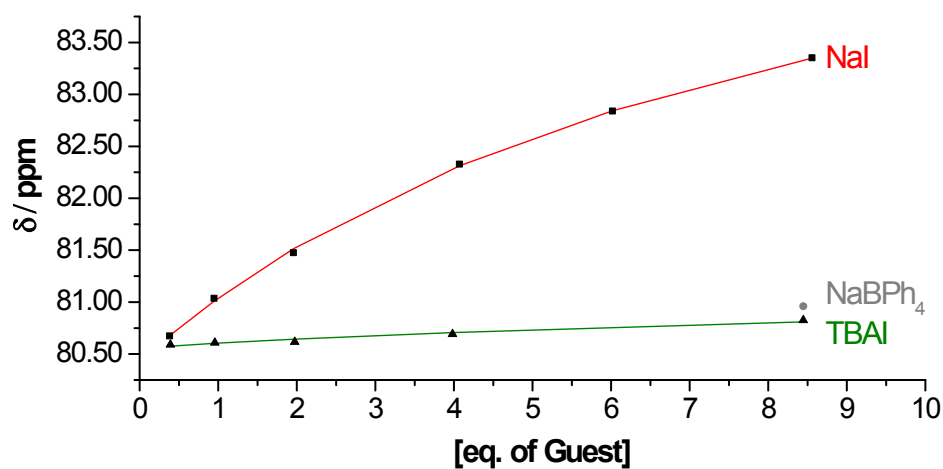


Figure S 38: Comparison of the chemical shift of C_{17} during the titration of 7 (1 mM stock solution) with NaI (red), TBAI (green) and NaBPh₄ (grey) in CD₂Cl₂:CD₃CN (3:1).

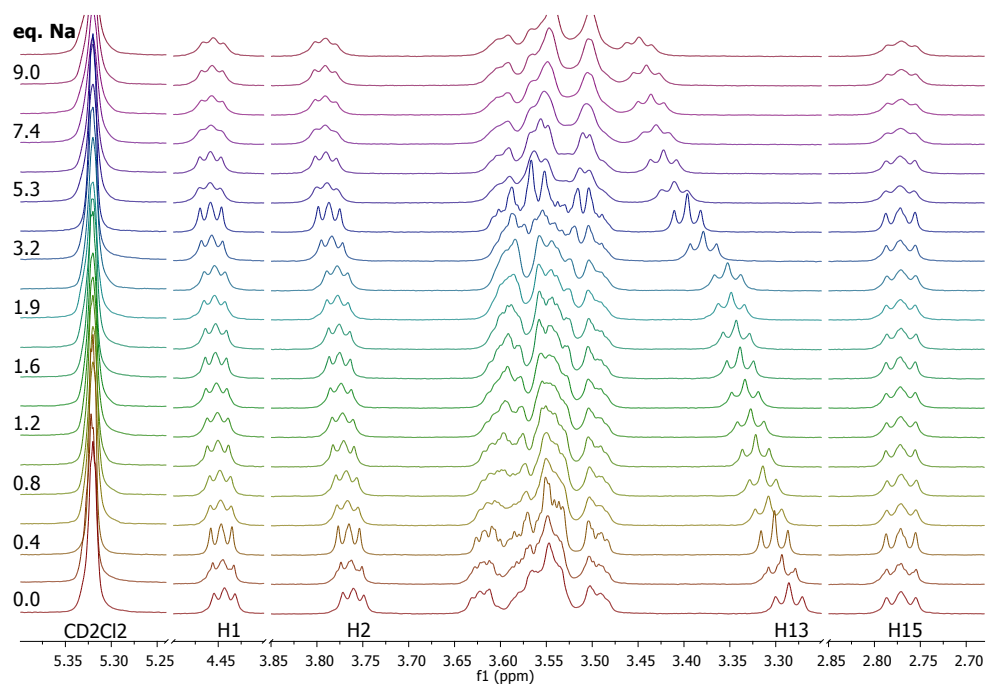


Figure S 39: ^1H NMR chemical shifts of **6** (2 mM stock solution) and NaBPh_4 (40 mM stock solution) in $\text{CD}_2\text{Cl}_2:\text{CD}_3\text{CN}$ (3:1).

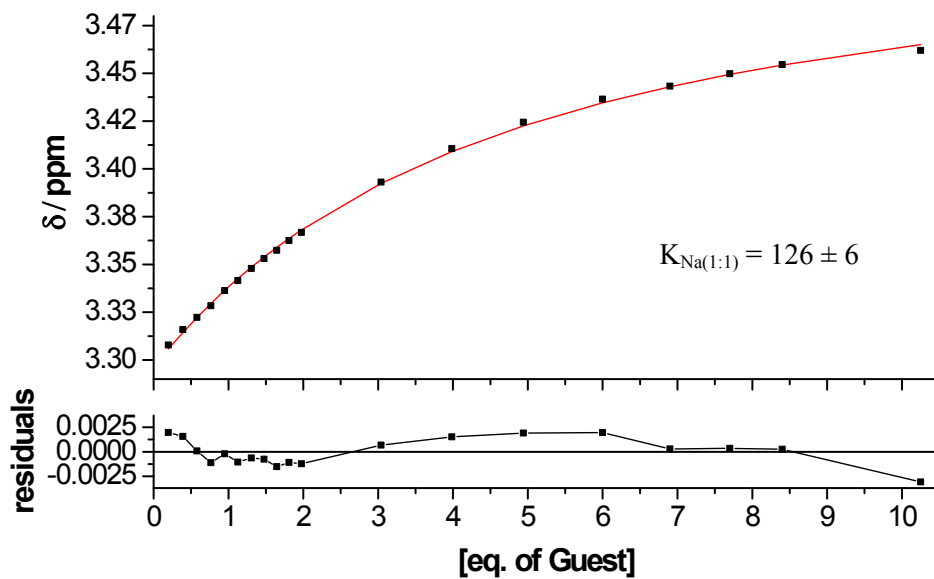


Figure S 40: Analysis of the binding isotherm (H_{13}) of **6** (2 mM stock solution) and NaBPh_4 (40 mM stock solution) in $\text{CD}_2\text{Cl}_2:\text{CD}_3\text{CN}$ (3:1) assuming a 1:1 (Host:Guest) binding model.

Since the HB based system **6** revealed an expected weaker anion binding affinity compared to the XB based system **7**, also the chemical shift decreased. As a result, the chemical shift of H₁₃ instead of H₁₅ had to be used to calculate the binding affinities for **6** (see **Figure S 39**). Unfortunately, a consistent calculation based on the chemical shift of H₁₃ for **6** and **7** was not possible due to the strong overlap of H₁₃ with other proton signals in the case of **7**. Nevertheless, comparing the binding affinity calculated *via* ¹H NMR titration of **6** × NaBPh₄ ($K_{\text{Na}} = 126 \pm 6 \text{ M}^{-1}$) with the ¹³C NMR titration of **6** × NaI ($K_{\text{Na}} = 174 \pm 30 \text{ M}^{-1}$), nearly the same cation affinities could be revealed which is in line with the results obtained for the XB based system **7**.

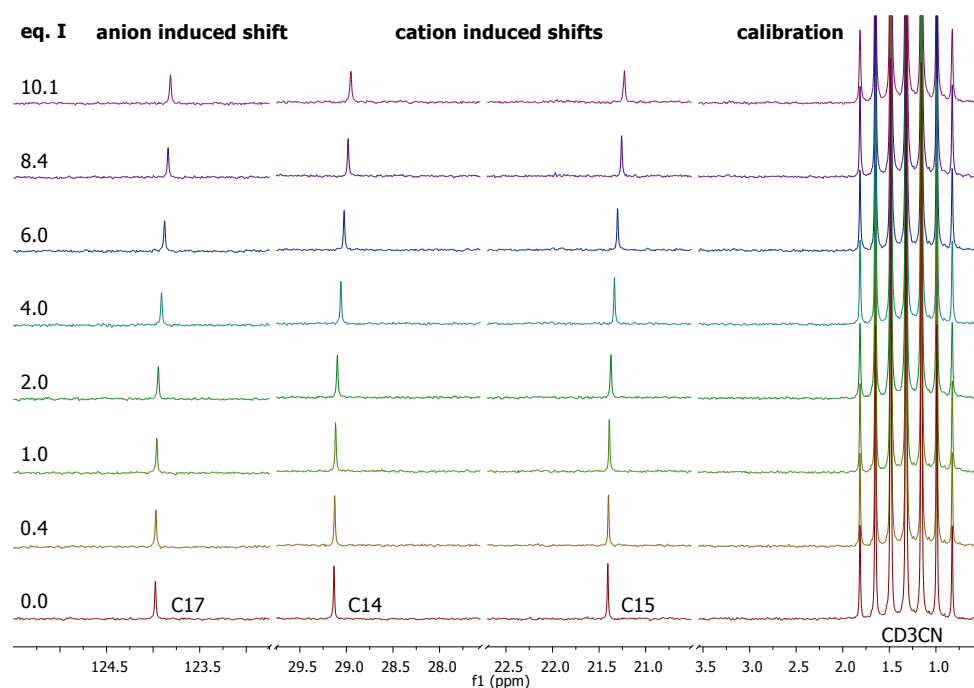


Figure S 41: ¹³C NMR chemical shifts of **6** (20 mM stock solution) and Bu₄NI (400 mM stock solution) in CD₂Cl₂:CD₃CN (3:1).

In case of the HB based system **6**, even a host concentration of 20 mM was not enough to create a sufficient chemical shift of the C₁₇ atom (0.16 ppm) to quantify the association constant (see **Figure S 41**). This observation is in line with the expected decrease of the binding affinity by changing from a XB to a HB based interaction.

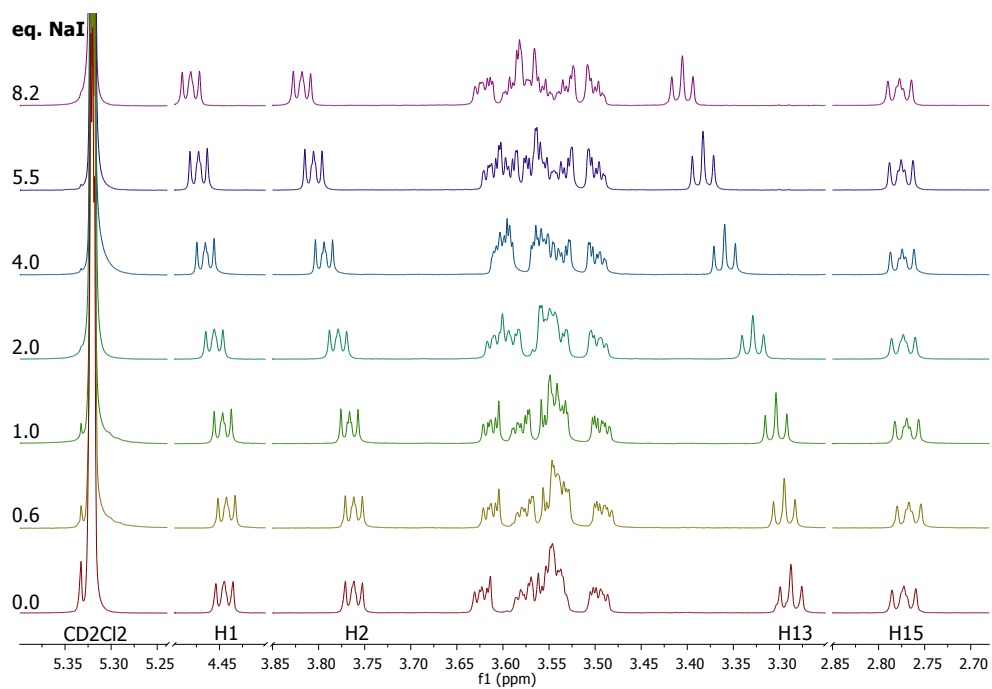


Figure S 42: ^1H NMR chemical shifts of **6** (1 mM stock solution) and NaI (20 mM stock solution) in $\text{CD}_2\text{Cl}_2:\text{CD}_3\text{CN}$ (3:1).

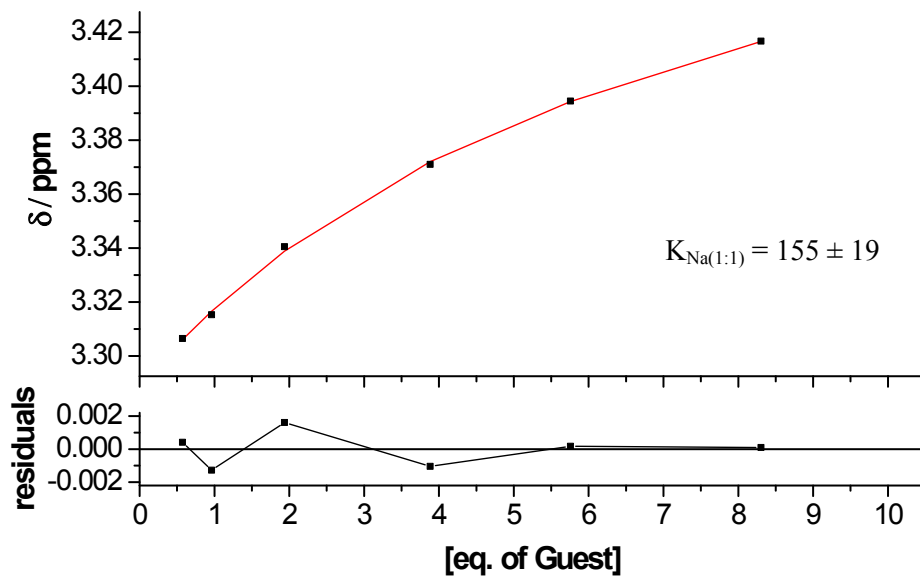


Figure S 43: Analysis of the binding isotherm (H_{13}) of **6** (1 mM stock solution) and NaI (20 mM stock solution) in $\text{CD}_2\text{Cl}_2:\text{CD}_3\text{CN}$ (3:1) assuming a 1:1 (Host:Guest) binding model.

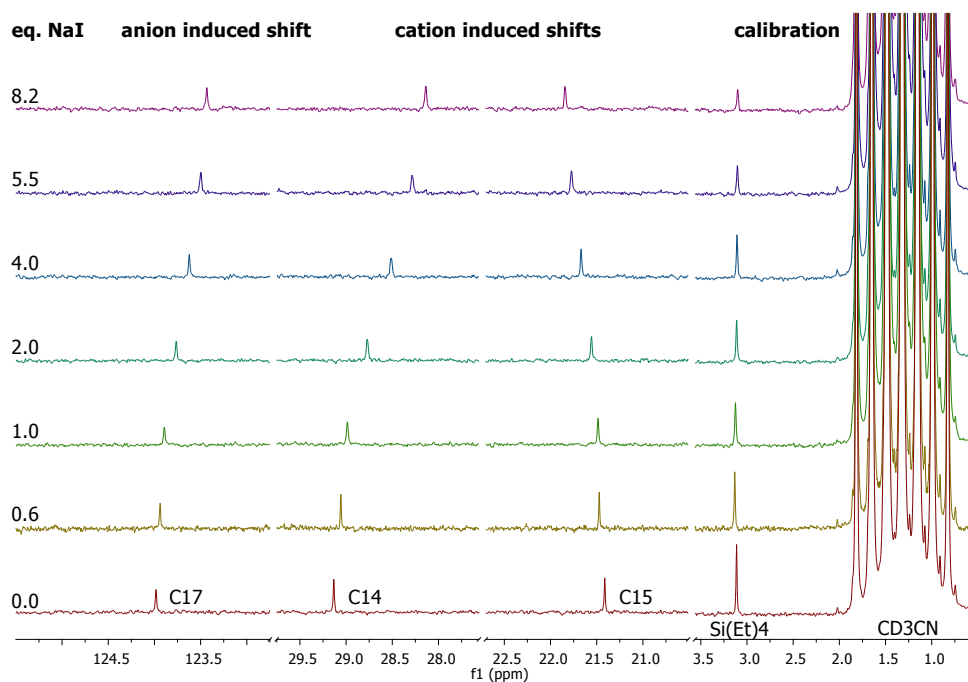


Figure S 44: ^{13}C NMR chemical shifts of **6** (1 mM stock solution) and NaI (20 mM stock solution) in $\text{CD}_2\text{Cl}_2\text{:CD}_3\text{CN}$ (3:1).

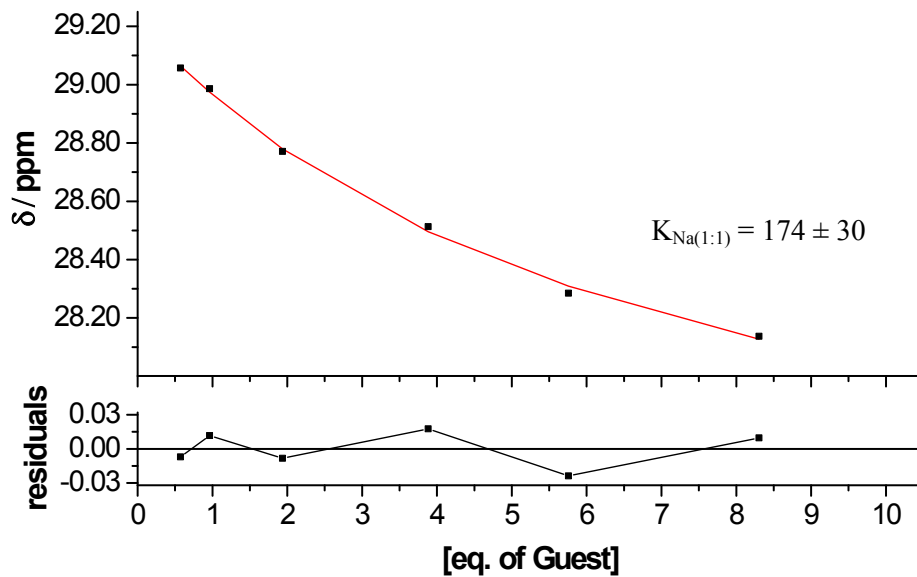


Figure S 45: Analysis of the binding isotherm (C_{14}) of **6** (1 mM stock solution) and NaI (20 mM stock solution) in $\text{CD}_2\text{Cl}_2\text{:CD}_3\text{CN}$ (3:1) assuming a 1:1 (Host:Guest) binding model.

Despite an observable shift of 0.55 ppm of the C₁₇ signal, a reliable quantification of the weak anion binding affinity K₁ in case of **6** × NaI was not possible. Here, the addition of significantly larger amounts of sodium iodide would have been necessary to achieve a reliable analysis of the binding isotherm, which was excluded due to solubility issues of the sodium salt. Noteworthy, instead of an expected downfield shift due to HB formation to the anion a highfield shift of the C₁₇ signal was observed. This highfield shift could be tentatively explained by breaking of an intramolecular HB through the addition of a sodium salt (**Figure S 46**), which would be in line with the solid state analysis (**Figure S 47**) as well as detailed ROESY experiments in solution (**Figure S 46**).

Selective ROESY experiments

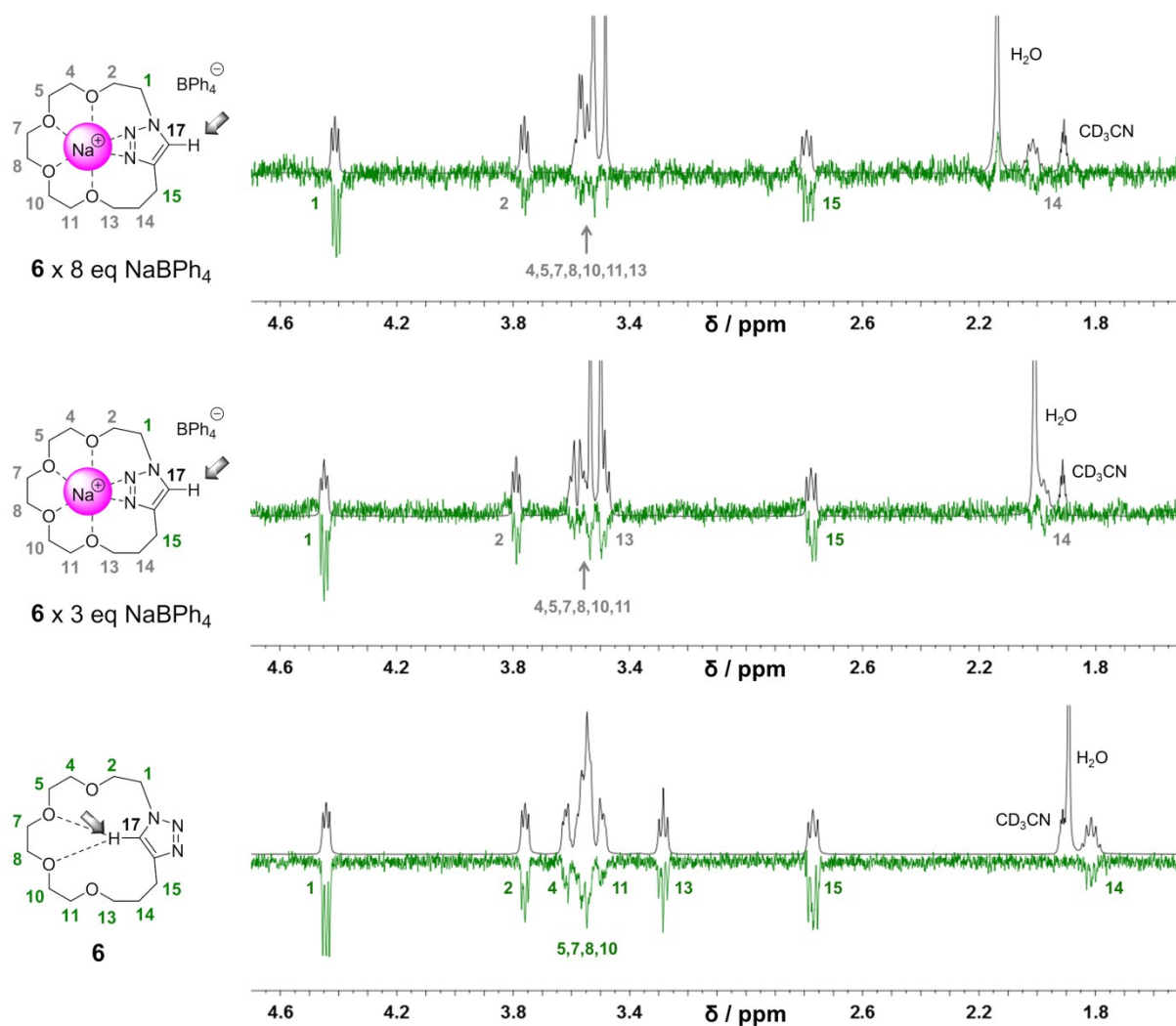


Figure S 46: NMR spectra and schematic representation of the ROE contacts; the selectively excited proton (H_{17}) is marked with a shaded arrow and strong as well as weak contacts are indicated with green and grey numbers, respectively. ^1H NMR (black) and selective ROESY spectra (green) for **6** [20mM] in the absence (bottom) as well as in the presence of 3 eq. (middle) and 8 eq. (top) of NaBPh_4 in a $\text{CD}_2\text{Cl}_2:\text{CD}_3\text{CN}$ (3:1) solvent mixture.

Comparing the cation binding affinities of **6** and **7**, a decreased K_{Na} for **6** was observable which was tentatively assigned to a possible intramolecular HB interfering with the cation complexation of the crown-ether. In this context, selective ROESY experiments of **6** were performed to clarify the existence of this intramolecular HB in a $\text{CD}_2\text{Cl}_2:\text{CD}_3\text{CN}$ (3:1) solvent mixture (see **Figure S 46**).

After excitation of the triazole proton (H_{17}) in the free macrocycle **6**, strong ROE signals to all protons of the crown-ether were observed. Thus, a free rotatable triazole moiety as well as a possible formation of an intramolecular HB between H_{17} and one of the oxygen atoms of the crown-ether was indicated (**Figure S 46** bottom).

In contrast, due to the addition of different equivalents of NaBPh_4 , the triazole moiety got involved in the complexation of the cation and, thus, its flexibility as well as the possibility for the intramolecular HB formation decreased (**Figure S 46** middle and top). Consequently, also the ROE signals to all protons located at the cation binding place decreased (H_2 to H_{13}), which was nicely underlined by a changed signal ratio concerning the neighboring protons (H_1 and H_{15}) and the more distanced protons (H_2 to H_{13}) (see **Table S 2**).

Table S 2: Ratio of the ROE signals with increasing amount of NaBPh_4 .

	$H_1/(H_4 \text{ to } H_{13})$	$H_{15}/(H_4 \text{ to } H_{13})$
6	0.42	0.37
6 × 3 eq NaBPh_4	0.89	0.56
6 × 8 eq NaBPh_4	1.24	0.83

Hence, the data is an indication for the formation of an intramolecular HB in the free macrocycle **6** which could be the reason for the decreased cation binding affinity of **6** compared to **7**. Moreover, this study in solution is in line with the observation of an intramolecular HB in the solid state (see **Figure S 47**).

4. Molecular structures:

Single crystals of **6** were obtained by slow vapor diffusion of *n*-pentane into a concentrated diethyl ether solution in the fridge (**Figure S 47**). Single crystals of **7** were obtained by slow vapor diffusion of *n*-pentane into a concentrated CH₂Cl₂ solution at room temperature (**Figure S 47**). Comparing the molecular structures of **6** and **7**, an intramolecular HB in case of **6** as well as an intermolecular XB in case of **7** is observable.

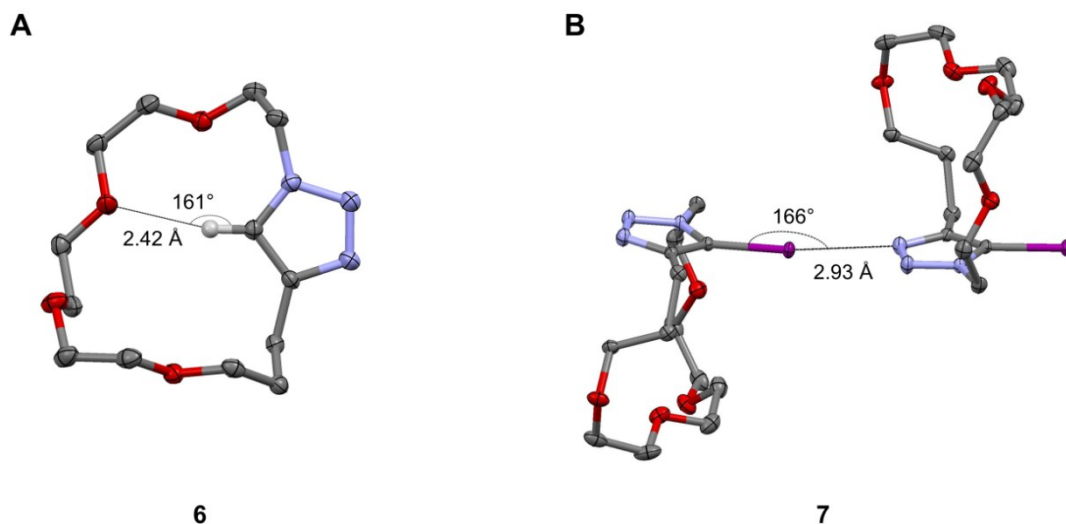


Figure S 47: Molecular structures of HB (A) and XB (B) based macrocycles **6** and **7** (thermal ellipsoids at 50% probability level, hydrogen atoms and solvent molecules are omitted for clarity; grey: carbon, blue: nitrogen, purple: iodine; and red, oxygen).

Compound **6** was dissolved in CH₂Cl₂ and an excess of NaPF₆ was added at room temperature. The resulting suspension was stirred at room temperature. After sedimentation, the clear solution was taken and single crystals of **6** with NaPF₆ were obtained by slow vapor diffusion of *n*-pentane into this concentrated CH₂Cl₂ solution (**Figure S 48**).

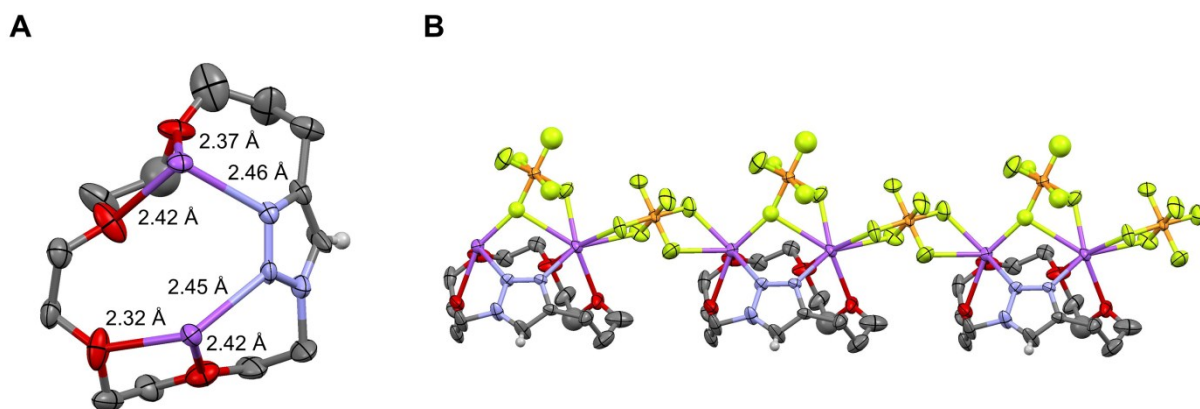


Figure S 48: Molecular structure of **6** interacting with NaPF₆ forming a 1:2 complex; top view of **6** without PF₆⁻ (A) as well as chain formation *via* bridging PF₆⁻ molecules (B) (thermal ellipsoids at 50% probability level, hydrogen atoms and solvent molecules are omitted for clarity; grey: carbon, blue: nitrogen, yellow: fluorine; orange: phosphorus; violet: sodium; and red, oxygen).

Equimolar amounts of **7** and NaBPh₄ were dissolved in a CH₂Cl₂/ethanol (3:2) mixture. Subsequently, single crystals of **7** with NaBPh₄ were obtained by slow vapor diffusion of *n*-pentane into this concentrated solution at room temperature (**Figure S 49**).

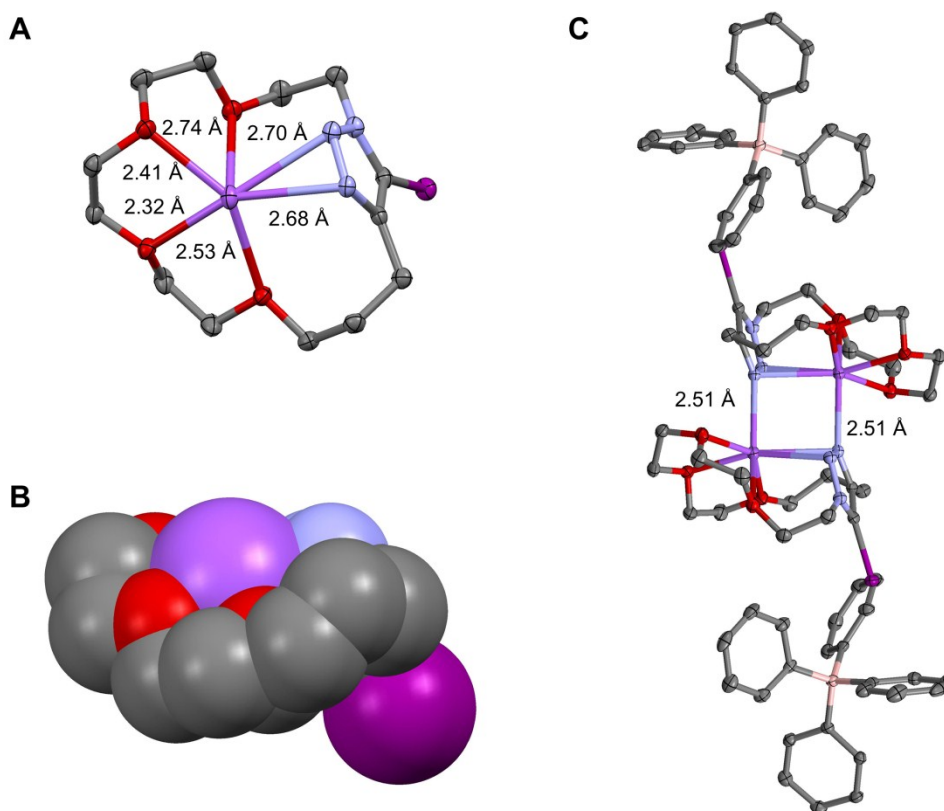


Figure S 49: Molecular structure of **7** interacting with NaBPh₄ forming a dimeric 1:1 complex; top view (**A**) and side view (**B**, space filled illustration mode) of **7** without BPh₄⁻ as well as dimer formation and connection to BPh₄⁻ (**C**) (thermal ellipsoids at 50% probability level, hydrogen atoms and solvent molecules are omitted for clarity; grey: carbon, blue: nitrogen, purple: iodine; pink: boron; violet: sodium; and red, oxygen).

Compound **7** (1 eq.) and a slight excess of NaI (1.3 eq.) were dissolved in a CH₂Cl₂/CH₃CN (4:1) mixture. Subsequently, single crystals of **7** with NaI were obtained by slow vapor diffusion of *n*-hexane into this concentrated solution at room temperature (**Figure S 50**).

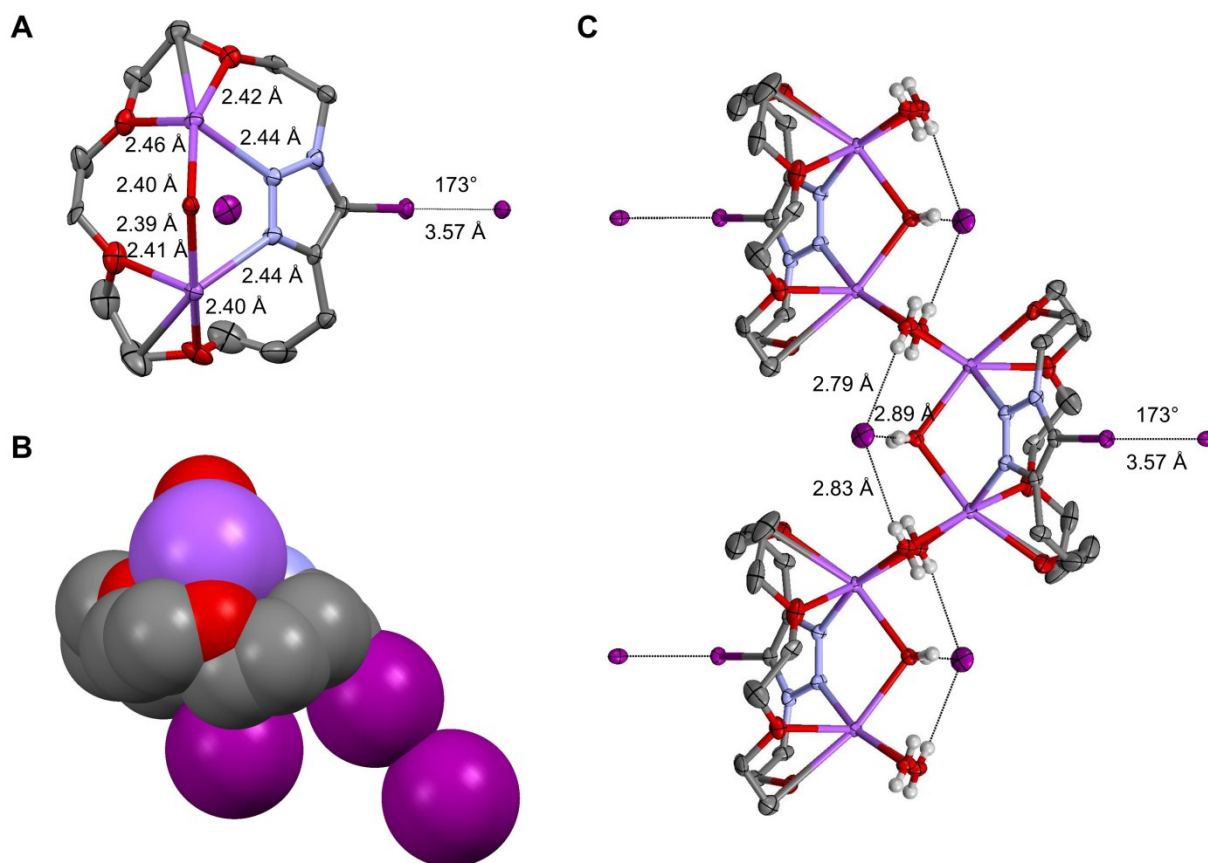


Figure S 50: Molecular structure of **7** interacting with NaI forming a 1:2 complex; top view (**A**) and side view (**B**, space filled illustration mode) of **7** interacting with sodium iodine as well as chain formation *via* bridging water molecules (**C**) (thermal ellipsoids at 50% probability level, hydrogen atoms and solvent molecules are omitted for clarity; grey: carbon, blue: nitrogen, purple: iodine; violet: sodium; and red, oxygen).

Crystallographic data (excluding structure factors) has been deposited with the Cambridge Crystallographic Data Centre as supplementary publication CCDC-1519088 for **6**, CCDC-1519089 for **6** × NaPF₆, CCDC-1519090 for **7**, CCDC-1519091 for **7** × NaBPh₄, and CCDC-1519092 for **7** × NaI. Copies of the data can be obtained free of charge on application to CCDC, 12 Union Road, Cambridge CB2 1EZ, U.K. E- mail: deposit@ccdc.cam.ac.uk.

Table S 3: Crystal data and refinement details for the X-ray structure determinations of the compounds.

Compound	6	6 × NaPF₆	7	7 × NaBPh₄	7 × NaI
Formula	C ₁₃ H ₂₃ N ₃ O ₄	C ₁₃ H ₂₃ F ₁₂ N ₃ Na ₂ O ₄ P ₂	C ₁₃ H ₂₂ IN ₃ O ₄	C ₇₄ H ₈₄ B ₂ I ₂ N ₆ Na ₂ O ₈	C ₂₆ H ₅₆ I ₆ N ₆ Na ₄ O ₁₄
fw (g·mol ⁻¹)	285.34	621.26	411.24	1506.87	1530.13
°C	-140(2)	-140(2)	-140(2)	-140(2)	-140(2)
crystal system	triclinic	monoclinic	monoclinic	monoclinic	monoclinic
space group	P $\bar{1}$	P 2 ₁	P 2 ₁ /n	C 2/c	P 2 ₁ /n
a/Å	4.6850(3)	9.6377(8)	8.5607(2)	19.2642(3)	11.5912(2)
b/Å	9.3425(8)	13.8800(9)	14.0000(3)	15.3487(3)	15.1724(3)
c/Å	17.3500(14)	10.0595(8)	14.2770(2)	25.2243(4)	14.1141(3)
α/°	90.082(5)	90	90	90	90
β/°	90.3350(7)	117.921(3)	106.910(1)	110.456(1)	90.364(1)
γ/°	104.252(3)	90	90	90	90
V/Å ³	736.01(10)	1189.03(16)	1637.11(6)	6988.0(2)	2482.15(8)
Z	2	2	4	4	2
ρ (g·cm ⁻³)	1.288	1.735	1.668	1.432	2.047
μ (cm ⁻¹)	96	3.4	19.75	9.72	38.48
measured data	2975	10800	12384	27745	27999
data with I > 2σ(I)	2493	3628	3602	7252	5194
unique data (R _{int})	2975/0.0667	4257/0.0697	3743/0.0198	7964/0.0360	5477/0.0362
wR ₂ (all data, on F ²) ^{a)}	0.2528	0.2759	0.0342	0.0547	0.0611
R ₁ (I > 2σ(I)) ^{a)}	0.0936	0.0966	0.0154	0.0260	0.0254
S ^{b)}	1.140	1.052	1.110	1.088	1.171
Res. dens./e·Å ⁻³	0.354/-0.387	1.094/-0.644	0.327/-0.293	0.362/-0.285	1.347/-1.805
Flack-parameter	-	0.2(3)	-	-	-
absorpt method	multi-scan	multi-scan	multi-scan	multi-scan	multi-scan
absorpt corr T _{min} /max	0.6393/0.7457	0.5025/0.7457	0.6981/0.7456	0.6949/0.7456	0.6105/0.7456
CCDC No.	1519088	1519089	1519090	1519091	1519092

^{a)} Definition of the *R* indices: $R_1 = (\sum ||F_o| - F_c|) / \sum F_o$;

$wR_2 = \{\sum [w(F_o^2 - F_c^2)^2] / \sum [w(F_o^2)^2]\}^{1/2}$ with $w^{-1} = \sigma^2(F_o^2) + (aP)^2 + bP$; $P = [2F_c^2 + \text{Max}(F_o^2)]/3$;

^{b)} $S = \{\sum [w(F_o^2 - F_c^2)^2] / (N_o - N_p)\}^{1/2}$.

5. Theoretical studies:

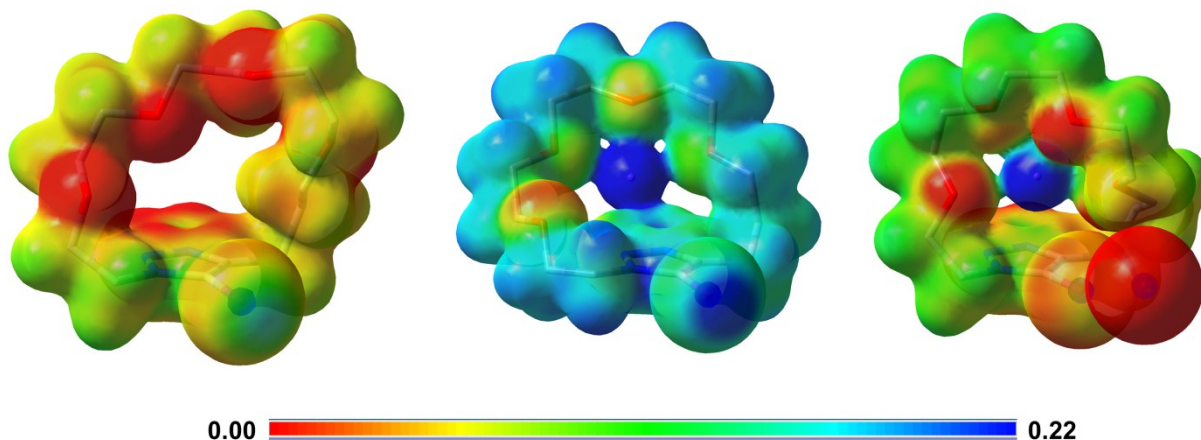


Figure S 51: Calculated molecular electrostatic potential surface (red: 0.00 to blue: 0.22) mapped on total density (isovalue 0.012) for **7** in the free (left), sodium complexed (middle) and sodium iodide complexed (right) form. Note that all electrostatic potential surfaces are plotted with the same parameters to warrant comparability.

For a better visualization of the influence of the cation complexation on the size of the σ -hole, electrostatic potential calculations were performed (**Figure S 51**). Comparing the data of the free (**left**) and the sodium complexed (**middle**) form, a significant increase in the size of the σ -hole due to an additional electrostatic force as well as an increased polarization of the 1,2,3-triazole moiety could be revealed.

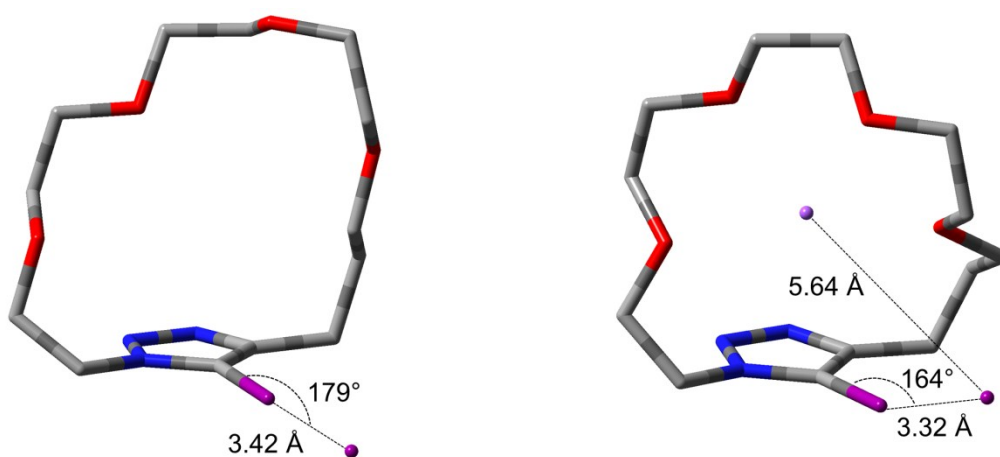


Figure S 52: Geometry optimized structures of **7** interacting with iodide (left) and sodium iodide (right).

Comparing the XB interaction of **7** and iodide with the interaction of **7** and sodium iodide (**Figure S 52**), the decreased XB length in case of the latter is in line with the cation induced activation of the host system and, thus, the detected stronger anion binding affinity calculated *via* NMR titration experiments.

7 (Figure S 49, left)				7...I (Figure S 50, left)			
SCF energy: -984.72784552 hartree				SCF energy: -996.22044134 hartree			
atom	x	y	z	atom	x	y	z
C	-3.70532	0.43152	0.1254	C	4.31897	2.43542	-0.39129
O	-3.63282	-0.25907	-1.14492	O	3.46618	3.16239	-1.30978
O	-2.032	2.16073	-0.0317	O	4.08056	0.10927	-0.95413
C	-3.4484	1.89701	-0.11843	C	4.91895	1.26934	-1.13763
O	0.6123	3.23207	-0.89831	O	2.54724	-2.38744	-1.81933
C	-0.30904	3.84627	0.03314	C	3.86508	-2.28284	-1.23283
C	-1.71498	3.51915	-0.39175	C	4.52885	-1.02175	-1.72408
N	1.96814	1.11225	0.5367	N	0.75297	-2.4772	0.50753
C	2.58339	1.91849	-0.51314	C	0.50529	-3.15863	-0.75522
C	2.00107	3.32001	-0.53139	C	1.80312	-3.56191	-1.43159
C	-4.1471	-1.60582	-1.1482	C	2.6006	4.14425	-0.70111
C	-3.07208	-2.61908	-0.83032	C	1.36542	3.52598	-0.08735
O	-2.62029	-2.45102	0.53381	O	1.7177	2.9284	1.18135
C	-1.22811	-2.07489	0.66089	C	0.87457	1.79885	1.523
N	1.52853	1.69827	1.68511	N	1.84616	-2.80513	1.26356
N	1.0111	0.74189	2.44372	N	1.84589	-1.98798	2.30981
C	1.11456	-0.46289	1.79183	C	0.76096	-1.1497	2.22666
C	1.72757	-0.22793	0.57701	C	0.0471	-1.46275	1.08029
C	-0.92052	-1.91159	2.13728	C	1.35095	1.21205	2.83733
C	0.58523	-1.71826	2.39117	C	0.54914	-0.05198	3.21103
H	-2.97268	0.03961	0.8307	I	-1.77985	-0.64952	0.32732
H	-4.70629	0.29191	0.54666	I	-4.71272	0.69186	-0.82101
H	-3.82672	2.16064	-1.1104	H	3.74799	2.07075	0.46123
H	-3.96752	2.50127	0.63445	H	5.10731	3.10848	-0.03564
H	-0.17264	4.93265	0.01942	H	4.99274	1.52734	-2.19871
H	-0.12781	3.46527	1.03961	H	5.92198	1.04483	-0.7546
H	-2.40188	4.20266	0.12228	H	4.4669	-3.14443	-1.54518
H	-1.82054	3.65612	-1.47172	H	3.79216	-2.2684	-0.14464
H	3.66364	1.95153	-0.36124	H	5.6148	-1.13018	-1.60426
H	2.37054	1.43742	-1.46589	H	4.3018	-0.8723	-2.78377
H	2.11817	3.79328	0.44372	H	-0.11681	-4.03963	-0.58362
H	2.53196	3.90665	-1.2826	H	-0.03905	-2.46823	-1.39695
H	-4.96678	-1.6976	-0.4286	H	2.39665	-4.18872	-0.76494
H	-4.53425	-1.78275	-2.15157	H	1.55924	-4.12441	-2.33448
H	-3.46598	-3.63177	-0.93765	H	3.1443	4.71589	0.05877
H	-2.23699	-2.48462	-1.52263	H	2.31021	4.81175	-1.51074
H	-0.5986	-2.86102	0.22785	H	0.5912	4.28422	0.06635
H	-1.04792	-1.1429	0.11199	H	0.98061	2.76118	-0.76782
I	2.26465	-1.56276	-0.93084	H	-0.16976	2.12195	1.59274
H	-1.26899	-2.80124	2.66408	H	0.94998	1.05673	0.72303
H	-1.46872	-1.05466	2.53318	H	1.25683	1.96209	3.62526
H	0.76622	-1.68154	3.46513	H	2.4075	0.95083	2.74481
H	1.13805	-2.5752	1.99689	H	0.86254	-0.39936	4.1958
				H	-0.51541	0.18911	3.26824

7...Na (Figure S 49, middle)				7...NaI (Figure S 49 + S 50, right)			
SCF energy: -1146.93105774 hartree				SCF energy: -1158.50876524 hartree			
atom	x	y	z	atom	x	y	z
Na	-1.99382	-0.25747	0.46987	Na	1.6196	0.68428	0.08623
C	-4.94988	-0.24011	-0.41963	C	2.23688	3.80517	0.54871
O	-3.77259	-1.04735	-0.64367	O	1.10197	2.94771	0.32982
O	-3.41658	1.56097	0.01338	O	3.52385	2.01525	-0.35388
C	-4.57354	1.17493	-0.77603	C	3.26431	3.43322	-0.48672
O	-0.79517	3.1201	-0.22332	O	3.03968	-0.37998	-1.64176
C	-1.91696	3.37348	0.65056	C	4.3991	0.01714	-1.32037
C	-3.18854	2.99794	-0.05956	C	4.45905	1.52008	-1.33752
N	1.30148	1.1662	0.45252	N	1.54815	-2.43164	-0.52244
C	1.52951	2.50197	-0.10758	C	1.64515	-2.31314	-1.96779
C	0.47289	3.47448	0.37114	C	2.96544	-1.66387	-2.32262
C	-3.95678	-2.47838	-0.54499	C	-0.03498	3.21131	1.19492
C	-2.63197	-3.10316	-0.89723	C	-0.82118	1.92948	1.25035
O	-1.64362	-2.61118	0.04383	O	0.05772	0.89511	1.79636
C	-0.35416	-3.29375	-0.07924	C	-0.48631	0.26534	2.994
N	0.1615	0.88928	1.13126	N	2.65716	-2.79592	0.19829
N	0.19901	-0.40362	1.45065	N	2.31489	-2.73114	1.4765
C	1.36038	-0.95917	0.98513	C	1.00303	-2.3238	1.57675
C	2.06973	0.04474	0.34592	C	0.50136	-2.12739	0.29918
C	0.4073	-3.26033	1.24885	C	0.4649	-0.78492	3.5454
C	1.67709	-2.39808	1.2062	C	0.34654	-2.18039	2.90454
H	-5.25522	-0.31501	0.62753	I	-1.37801	-1.29145	-0.31558
H	-5.76919	-0.57977	-1.0576	I	-3.93717	0.76162	-0.84627
H	-4.3219	1.24848	-1.83586	H	2.62689	3.64509	1.55783
H	-5.40912	1.84442	-0.55652	H	1.95481	4.85511	0.43418
H	-1.95576	4.43633	0.90526	H	2.87749	3.63224	-1.48938
H	-1.8063	2.7913	1.57021	H	4.18681	3.99899	-0.33304
H	-4.03725	3.50138	0.40955	H	5.09141	-0.37533	-2.06853
H	-3.12291	3.3003	-1.10713	H	4.66532	-0.3901	-0.34293
H	2.51804	2.83966	0.20317	H	5.46836	1.86675	-1.10072
H	1.50476	2.42867	-1.19504	H	4.17042	1.88957	-2.32534
H	0.40416	3.44407	1.46037	H	1.57363	-3.29535	-2.43533
H	0.75478	4.4816	0.06047	H	0.80779	-1.70672	-2.30954
H	-4.25296	-2.74464	0.47287	H	3.78586	-2.29573	-1.98482
H	-4.72836	-2.80567	-1.24556	H	3.03358	-1.50434	-3.39956
H	-2.70411	-4.19063	-0.82147	H	0.32823	3.48386	2.19012
H	-2.344	-2.83211	-1.91579	H	-0.63314	4.02489	0.78153
H	-0.55316	-4.32431	-0.37923	H	-1.71557	2.03727	1.8652
H	0.21455	-2.81248	-0.88107	H	-1.15967	1.62864	0.25864
I	3.91563	-0.02274	-0.60938	H	-0.64555	1.05455	3.73478
H	0.68927	-4.27377	1.53248	H	-1.45515	-0.17677	2.7435
H	-0.26959	-2.8903	2.01865	H	0.24869	-0.88499	4.6118
H	2.22373	-2.5126	2.14521	H	1.49228	-0.42004	3.46697
H	2.3434	-2.74792	0.41405	H	0.80948	-2.90921	3.57053
				H	-0.70978	-2.44735	2.81987

6. References:

- (1) Brummond, K. M.; McCabe, J. M. *Tetrahedron* **2006**, *62*, 10541.
- (2) Nonius, B. V.; *COLLECT*, Netherlands, **1998**.
- (3) Otwinowski, Z.; Minor, W. In *Methods Enzymol.*; Charles W. Carter, Jr., Ed.; Academic Press: **1997**; Vol. 276, p 307.
- (4) Sheldrick, G. SADABS, version 2.10, Bruker-AXS, Inc.: Madison, WI, **2002**.
- (5) Sheldrick, G. *Acta Cryst. A* **2008**, *64*, 112.
- (6) Sheldrick, G. *Acta Cryst. C* **2015**, *71*, 3.
- (7) Spek, A. *Acta Cryst. C* **2015**, *71*, 9.
- (8) Frisch, M. J. Revision A.02 ed.; Gaussian, Inc.: Wallingford, CT, **2010**.
- (9) Zhao, Y.; Truhlar, D. *Theor. Chem. Acc.* **2008**, *120*, 215.
- (10) Weigend, F.; Ahlrichs, R. *Phys. Chem. Chem. Phys.* **2005**, *7*, 3297.
- (11) Dennington, R. D.; Keith, T. A.; Millan, J. M.; Version 5.0.8 ed.; Semicchem, Inc.: Wallingford, CT, **2008**.
- (12) Binauld, S.; Hawker, C. J.; Fleury, E.; Drockenmuller, E. *Angew. Chem. Int. Ed.* **2009**, *48*, 6654.
- (13) Hynes, M. J. *Chem. Soc., Dalton Trans.*, **1993**, *2*, 311.